chemosensors

MDPI

Review

Advances and Perspectives in Chemical Imaging in Cellular Environments Using Electrochemical Methods

Robert A. Lazenby [1] and Ryan J. White [1,2,*]

[1] Department of Chemistry, University of Cincinnati, Cincinnati, OH 45219, USA; lazenbra@ucmail.uc.edu
[2] Department of Electrical Engineering and Computer Science, University of Cincinnati, Cincinnati, OH 45219, USA
* Correspondence: ryan.white@uc.edu; Tel.: +1-513-556-4837

Received: 23 April 2018; Accepted: 23 May 2018; Published: 29 May 2018

Abstract: This review discusses a broad range of recent advances (2013–2017) in chemical imaging using electrochemical methods, with a particular focus on techniques that have been applied to study cellular processes, or techniques that show promise for use in this field in the future. Non-scanning techniques such as microelectrode arrays (MEAs) offer high time-resolution (<10 ms) imaging; however, at reduced spatial resolution. In contrast, scanning electrochemical probe microscopies (SEPMs) offer higher spatial resolution (as low as a few nm per pixel) imaging, with images collected typically over many minutes. Recent significant research efforts to improve the spatial resolution of SEPMs using nanoscale probes and to improve the temporal resolution using fast scanning have resulted in movie (multiple frame) imaging with frame rates as low as a few seconds per image. Many SEPM techniques lack chemical specificity or have poor selectivity (defined by the choice of applied potential for redox-active species). This can be improved using multifunctional probes, ion-selective electrodes and tip-integrated biosensors, although additional effort may be required to preserve sensor performance after miniaturization of these probes. We discuss advances to the field of electrochemical imaging, and technological developments which are anticipated to extend the range of processes that can be studied. This includes imaging cellular processes with increased sensor selectivity and at much improved spatiotemporal resolution than has been previously customary.

Keywords: SEPM; SECM; SICM; biosensors; high-resolution imaging; ion channels; microelectrode arrays

1. Introduction

Chemical imaging using electrochemical techniques chiefly comprises scanning electrochemical probe microscopies (SEPMs). SEPM is made up of a selection of techniques that broadly fall into the two categories of scanning electrochemical microscopy (SECM) and scanning ion conductance microscopy (SICM). Numerous modes and sub-techniques, bringing a wealth of accompanying acronyms, have evolved as a means to add capability to these principle imaging techniques. This review article addresses the means to bring improved chemical selectivity to electrochemical imaging, with an emphasis on advances in the field within the last five years (2013–2017). Citations of earlier significant works are included where relevant.

Electrochemical imaging using SEPM employs a scanned probe, with a critical dimension for imaging on the micro- or nanoscale. This size scale allows the measurement of activity heterogeneity across a surface, gaining additional insights over bulk electrochemical methods, for which a response arises from average current over the whole surface. In addition, other surface properties can be

mapped using SEPM and complementary techniques, such as surface morphology, sample conductivity, and atomic force between probe and sample. Scanning electrochemical microscopy has been extensively and recently reviewed [1–3], notably for living cells [4] and in neuroscience [5]. Other SEPM reviews include multifunctional probes for SICM [6], nanoscale electrochemical imaging [7–9], and the use of tip integrated biosensors [10]. This review makes an emphasis of probe geometries, given that the size, shape, and functionality of the probe dictates what type of imaging can be achieved and the resolution that is attainable. The key probes discussed in this review are represented by the schematics in Figures 1 and 2, with labels stating the section of this review in which they are discussed. Note that not all modes or variants of each technique are shown and probe geometries are representative of those used in the techniques described.

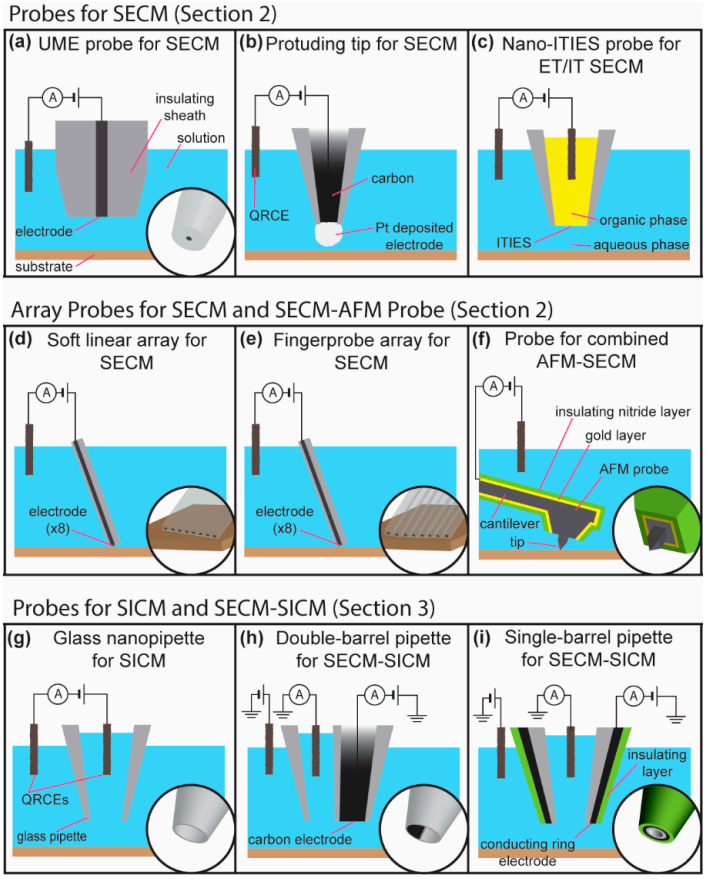

Figure 1. Schematics showing cross-sections of various probes typically used in scanning electrochemical probe microscopies (SEPM) experiments in typically used configurations (with a quasi-reference counter electrode (QRCE) such as Ag/AgCl). Insets show a 3D view of the probe, for clarity. (**a**) Ultramicroelectrode (UME) probe for use in scanning electrochemical microscopy (SECM), shown for the feedback mode. (**b**) A single barrel glass pipette filled with pyrolyzed carbon, and Pt electrodeposited directly onto the carbon can form a planar Pt electrode or a more protruding Pt electrode, with increased deposition time/current. (**c**) A nanopipette-supported interface between two immiscible electrolyte solutions (ITIES) can be used for SECM. (**d**) Soft linear array probe (typically eight electrodes) for SECM. (**e**) Finger probe electrode array, which differs from the soft linear array probe by the separation between electrodes to allow independent topographical movement of each electrode. (**f**) A combined SECM-atomic force microscopy (AFM) probe. (**g**) Single barrel glass nanopipette, filled with electrolyte solution, used for scanning ion conductance microscopy (SICM). (**h**) A double barrel glass pipette, with one barrel filled with pyrolyzed carbon for use as an SECM electrode and the second barrel filled with electrolyte solution for use as an SICM probe, in a combined SECM-SICM probe. (**i**) A combined SECM-SICM probe produced from a single barrel glass pipette.

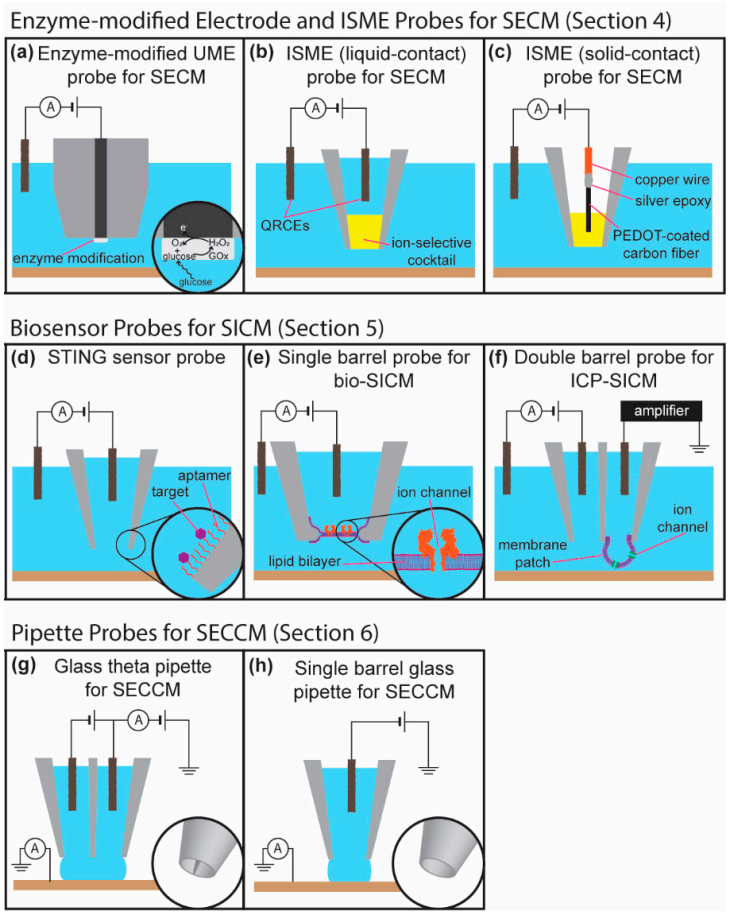

Figure 2. Schematics showing cross-sections of functional probes and droplet-based probes used in SEPM experiments. Insets show either a zoom-in view of the sensing part of biosensor probes or a 3D view of the probe, for clarity. Note that these schematics are not to scale, and configurations are examples of those typically used (with a quasi-reference counter electrode (QRCE) such as Ag/AgCl). Insets show 3D view of the probe, for clarity (**a**) An ultramicroelectrode (UME) can be modified with an enzyme, by electropolymerization or dropcasting, to give chemical specificity to the probe for use in SECM. Inset shows the mechanism of glucose detection using a glucose oxidase (GOx) enzyme layer. (**b**) Ion selective microelectrode (ISME) with a liquid-contact connection. (**c**) ISME with a solid-contact connection. (**d**) A glass nanopipette functionalized with an aptamer to produce a signal transduction by ion nanogating (STING) sensor. (**e**) Single glass pipette filled with electrolyte solution with a suspended lipid bilayer at the tip opening, into which protein ion channels may be reconstituted, used for bio-inspired (bio)-SICM. (**f**) A dual barrel glass pipette, in which both barrels are filled with electrolyte solution and one barrel supports a lipid membrane which has ion channel(s) incorporated, for use as an ion channel probe (ICP) and the second barrel functions as an SICM probe. (**g**) Double barrel theta glass pipette, with both barrels filled with electrolyte solution, connected by a meniscus at the pipette opening that creates an electrochemical cell at the substrate surface, used for scanning electrochemical cell microscopy (SECCM). (**h**) Single barrel glass pipette, filled with electrolyte solution, connected by a meniscus at the pipette opening that creates an electrochemical cell when in contact with the substrate surface, used for SECCM.

Noteworthy additions to the SEPM literature in the last five years include the application of novel and multifunctional electrochemical imaging probes, pushing the limits of spatial resolution with nanoscale electrochemical imaging, and producing activity movies, where the means of acquiring an image does not necessarily require the use of a constant applied potential. The last five years has seen the introduction of several techniques that add chemical selectivity to electrochemical imaging,

particularly in the growing field of biosensors. This review elaborates on the possibility of combining miniaturized biosensor platforms with high-resolution imaging techniques and methods of using nanoscale and microscale biosensors amenable to SEPM, even if their full potential is yet to be realized. This includes signal transduction by ion nanogating sensors, ion channel probes, and electrochemical aptamer-based sensors.

Finally, this review discusses non-scanning techniques employing microelectrode arrays (MEAs) that typically allow for much higher temporal resolution than SEPM, where whole frames of an image can be mapped in a few milliseconds (ms). Moreover, each pixel (i.e., electrode in an array device) is measuring simultaneously, as opposed to a mobile scanned probe which can only make measurements at one position at once. However, due to device fabrication restrictions and the potential for electrode cross-talk for electrodes with small separation distances, MEAs have much lower spatial resolution for imaging. This review will cover chemical imaging using electrochemical imaging methods, offer future perspectives that could be realized with the implementation of recently developed biosensor probes in SEPM, and discuss imaging using electrode array-type platforms for spatially resolved chemical measurements in real time.

2. Scanning Electrochemical Microscopy

Scanning electrochemical microscopy, pioneered concurrently by Bard and coworkers [11] and Engstrom and coworkers [12], is a powerful electroanalytical tool to quantitatively study the local electroactivity of a surface [13]. Applications include the areas of corrosion science [14], crystal dissolution [15], biological permeability [16], enzyme activity [17,18], and kinetic rate studies. The technique employs a scanned probe with an active electrode radius of micro- to nanometer dimensions, referred to as an ultramicroelectrode (UME) [19]. The probe electrode is scanned or positioned over a substrate of interest to build an image of electroactivity and topography. The smaller the active electrode radius, and the closer it is to the substrate, the higher the attainable spatial resolution for imaging.

Redox-active molecules may be directly detected using an applied potential to oxidize or reduce the molecule at the probe electrode. Chemical specificity is achieved by the proper selection of a potential to oxidize or reduce the molecule of interest, which is convenient if few redox species are present. In the amperometric feedback mode of SECM, a redox-active species is artificially added to the solution, and the current at the tip electrode provides information on both the conductivity and topography of the underlying substrate.

The steady-state current in bulk solution (far away from the substrate) is a result of the hemispherical diffusion of species to the UME. In close proximity to an insulating substrate, this diffusion is hindered and the current measured at the tip electrode is smaller than in bulk, termed negative feedback. When the probe is positioned over conducting substrate, the current at the tip is higher than in bulk, due to regeneration of the redox species at the substrate surface, termed positive feedback. The current measured at the tip electrode is affected by both the tip-substrate separation distance and the conducting nature of the underlying substrate, (i.e., topographical and electroactivity effects of the substrate are convoluted in the tip current). These may be deconvoluted using a method that determines the tip-substrate distance, which can be used as a feedback mechanism for distance control during imaging of a substrate (vide infra). There are many modes of SECM, such as the feedback mode discussed [20], generation collection modes [21], redox competition mode [22], surface interrogation mode [23], direct mode [24], potentiometric mode [25], and fast-scan cyclic voltammetry (FSCV) mode [26]. The advantages and applications of these and other modes are described elsewhere and are not the focus of the present manuscript.

2.1. Constant-Distance Imaging Modes

Scanning the probe at a fixed height, not accounting for changes in topography of the substrate, is termed constant-height mode. A significant challenge of SECM is that the measured amperometric tip

current is a convolution of electrochemical activity and tip-substrate separation distance, which changes due to surface morphology. To overcome this, there has been much effort to introduce feedback mechanisms that take into account surface morphology and sample tilt to enable constant-distance imaging, (i.e., where the tip-substrate separation distance is kept constant through the scan by continuous readjustment of the height (z-position)). Furthermore, a feedback mechanism that allows constant-distance imaging also enables the tip to be placed closer to the sample surface without the possibility of tip-crash.

Methods of tip-substrate distance regulation for SECM [27] include simply using the faradaic current, the use of impedance in alternating current (AC)-SECM [28], the use of oscillating probes in tip-position modulation (TPM)-SECM [29], shear-force SECM [30], intermittent contact (IC)-SECM [31], and three-dimensional super-resolution optical imaging [32]. There are advantages and limitations to each of these techniques, for example the faradaic current is somewhat limited by the fact that the current response at an electrode is affected by both the tip-substrate separation distance and the electroactivity of the underlying substrate. Alternating current-SECM uses impedance, and thus, relies on an electrochemical signal for feedback which could change during a scan, and TPM may require additional models that take into account the nature (i.e., permeability and conductivity) of the underlying substrate [33]. On the other hand, IC and shear-force SECM rely on a non-electrochemical signal for tip-positioning, so they are less susceptible to changes in the solution during the scan. Intermittent contact relies on physical contact between the tip and substrate, thus it occludes soft samples, which makes shear-force a more promising candidate for imaging cells.

As novel sensor and biosensor platforms become integrated with SECM, which may not use an amperometric current, a means of sensor positioning becomes more challenging [10]. Shear-force has been widely adopted as a non-electrochemical and non-contact method to assign tip-substrate separation [34,35]. In this method of non-contact distance regulation, the tip is oscillated in resonance laterally using a small amplitude (from below 1 nm up to 5 μm), and distance-dependent shear-forces are used to maintain a constant tip-substrate separation. Close to the surface, up to maximum distances of a few hundred nanometers, hydrodynamic shear-forces impede the free lateral movement of the tip, and the amplitude of the vibrating tip is used for distance feedback.

There are also combined techniques such as SECM-SICM [36,37] and SECM-atomic force microscopy (AFM) [38]. These multifunctional probes are attractive given that they have separate components for independent and deconvoluted measurement of electroactivity and topography. SECM-SICM for example uses the SICM component of the probe as a means of achieving distance control for topography, with simultaneous measurement of an electrochemical signal using the SECM component of the probe, and is discussed in greater detail in Section 3 (vide infra). Although SECM-SICM and SECM-AFM require specialized probes (Figure 1), these are becoming more widely adopted [39]. For example, SECM-AFM probes are now commercially available, and SECM-SICM probes can be fabricated in minutes at low cost (excluding the large initial cost of a laser-based pipette puller). Using SECM-AFM to image soft cellular samples can be problematic due to the nature of feedback of AFM in which tip-sample contact is made throughout the image, whereas SECM-SICM probes do not make contact with the substrate making them a non-destructive probe [40].

AFM is capable of very high spatial resolution (i.e., sub-nm topography and lateral resolution governed by the probe shape). SECM-AFM uses a probe that has topographical resolution based on the size and shape of the sharp AFM tip and electrochemical imaging resolution based on the geometry of the surrounding electrode (Figure 1f). This technique has been used to study ionic diffusion at nanopores, simultaneously with electrochemical currents associated with flux of species through the pores (SECM) and the pore topography/spacing (AFM) [41].

2.2. Scanning Electrochemical Microscopy Using Microelectrode Array Probes

There are examples of combining SECM and MEAs, that involve using a linear array as a scanned probe [42,43]. Single soft probes were developed by Girault and coworkers (for antioxidant mapping) [44] that were capable of tracing the contours of a soft surface. These probes were developed into soft linear array probes, in an approach that allows scanning over a large area in a shorter time than for a single electrode probe to achieve high-throughput imaging (Figure 1d) [45]. A disadvantage of using a linear array as a scanned probe is that given a topographically varied site, each electrode will be at a slightly different tip-substrate separation distance during the scan. A means to overcome this is to use a finger-probe (FP) MEA (Figure 1e), in which each electrode in the array traces the topography independently of its neighboring electrodes [46], or spider-probes, which operate on the same principle [47].

2.3. Nanoscale Imaging Using SECM

A long-term trend in SECM technologies has been the production and implementation of smaller probes, leading to nanoimaging for high resolution (HR)-SECM [48]. The benefits of using nanoelectrodes are to increase the mass transport to the electrode, due to increased diffusion that follows a hemispherical field around the electrode, smaller resistance-capacitor (RC) time constants and low ohmic drops, and to obtain higher spatial resolution images. The radius of a disk electrode will determine the resolution achievable as well as the distance it is from the substrate, meaning distance feedback is required for super-high-resolution imaging with nanoelectrodes.

When working with probes that have critical electrode dimensions on the nanoscale, special care should be taken to avoid probe damage caused by electrostatic discharge (ESD) [49]. This has also been reported for nanopipette-supported pyrolytic carbon tips [50]. Local relative humidity may explain why such effects are not always reported, since increased humidity will help to reduce ESD events, which may result in unintended ESD protection. Another consideration for nanoscale imaging is the effect of temperature changes on the piezoelectric positioners that control tip movement. An isothermal chamber can be used to suppress the thermal drift of positioners that may occur over long periods of image acquisition [51]. When such appropriate measures are taken to ensure a stable tip-substrate nanogap, nanometer scale SECM imaging is feasible [52]. A nanometer-sized tip, for example, allowed imaging of single 10 or 20 nm gold particles [53]. This size tip also allows studies of the electrocatalytic activity of individual Pt nanoparticles [54].

An interesting development in nanoscale SECM is the use of a nanopipette-supported interface between two immiscible electrolyte solutions (ITIES). Shigeru and coworkers [55] used a 30 nm diameter probe (silanized quartz nanopipette) filled with 1,2-dichloroethane (DCE) to produce a nanoscale ITIES, and used this to image a nanoporous Si_3N_4 membrane. The ITIES protruded from the tip of a nanopipette, in a sphere-cap geometry [16], which did not significantly compromise spatial resolution, in part due to the fact that the tip could be scanned closer to the substrate. Mirkin and coworkers [56] recently introduced the electron transfer/ion transfer (ET/IT) mode of SECM (Figure 3), which also utilizes ITIES. In their approach, a nanopipette is filled with an organic liquid phase (e.g., DCE) to form an ITIES at the tip opening (Figure 1c). A neutral redox species that is sufficiently soluble in both the aqueous and organic phases (e.g., ferrocenedimethanol (FDM)) is placed initially inside the pipette. Over the course of the experiment, the redox species partitions from the organic phase to the aqueous phase, and thus, can be delivered to the surface during the experiment in close proximity to a conducting substrate (within a few tip radii), and the redox species FDM can diffuse to and oxidize at the surface. The oxidation current measured represents the local ET rate beneath the tip. The product of this reaction at the surface, FDM^+, can diffuse into the pipette by application of an applied (negative) potential in the electrode within the pipette, which results in an IT tip current. As described, this is referred to as positive IT feedback, since negative IT feedback would refer to a reduction reaction at the substrate surface (Figure 3a). The initial absence of (potentially toxic) redox mediator in bulk solution, as well as the high spatial resolution, make this a suitable mode to study

biological cells. The ET/IT was shown with proof-of-concept images, including substrate reactivity mapping arising from the oxidation of FDM at a Pt substrate (Figure 3).

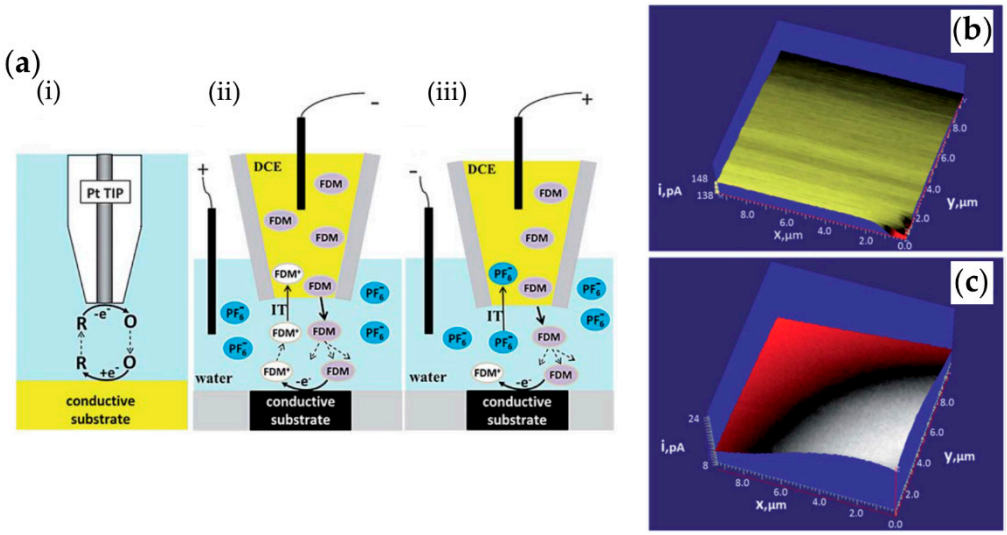

Figure 3. Electron transfer/ion transfer (ET/IT) mode of SECM for imaging a 12.5 μm radius Pt disk substrate. External (aqueous) solution contains 1 mM $LiPF_6$, and the pipette is filled with 26 mM ferrocenedimethanol (FDM) in 1,2-dichloroethane (DCM) (organic). (**a**) Schematics of (i) the feedback mode of SECM in which a reduced species (R) is oxidized at the Pt tip electrode to form the oxidized species (O) that can be reduced at the conducting substrate beneath the tip; (ii) the ET/IT mode with positive IT feedback; and (iii) the ET/IT mode with negative IT feedback. (**b**) Topography image of the substrate, produced by the negative IT current of PF_6^- IT, shows no features. (**c**) Substrate reactivity map arising from oxidation current of FDM partitioning from the filling solution. (Adapted from Reference [56] with permission of The Royal Society of Chemistry).

3. Scanning Ion Conductance Microscopy

Scanning ion conductance microscopy (SICM) was first introduced by Hansma et al. in 1989 [57]. Scanning ion conductance microscopy uses the ion current between two quasi-reference counter electrodes (QRCEs) as a feedback mechanism for high resolution topographical imaging, where one electrode is placed inside a small (tens to hundreds of nm) pipette and the other is placed in the external bathing electrolyte solution (Figure 1e). The method is predicated on measuring probe-substrate separation distance dependent changes in ionic current to map topographical features of the surface. The lateral resolution of SICM depends on the pipette inner opening radius, r_i, where the fundamental limit of resolution can be approximated to $3r_i$, as a useful rule-of-thumb for the minimum resolvable object distance [58]. Even so, features smaller than the fundamental limit and smaller than r_i, can be detected, and so values smaller than this limit can be found in the literature. The $3r_i$ limit was obtained using the full width at half maximum (fwhm) of the special point spread function (sPSF) of the SICM, which gives a more meaningful value than using the separation between the closest edges to two resolved objects [58].

Scanning ion conductance microscopy, as a contact-free SPM, is particularly attractive for its use in imaging living cells by avoiding cell deformation, which could occur using AFM, where tip-sample contact is unavoidable (in standard imaging modes) [40]. Live cells have been imaged by SICM, and exceptionally high resolution imaging (comparable to scanning electron microscopy) of the 3D surfaces of tissues have been imaged using hopping mode scans (vide infra) [59], although obtaining chemical information is not trivial. In the traditional sense, SICM does not provide any chemical information. More recently, SICM as a standalone technique has been used to image ion flux that arises from (electro)chemical reactions at an interface [60]. This is a recent advance that is not directly

chemical imaging, but allows for probing of a reaction of interest at an interface by monitoring changes in local conductivity at a surface. Information can be inferred about chemical reactions at a surface, since chemical transformations result in ion fluxes that will influence the ionic current flowing through the nanopipette imaging probe. Surface charge of a substrate can also be mapped using SICM, given that there is an interaction of the diffuse double layers of the nanopipette and the substrate surface [61]. The ion current is dependent on the polarity of the applied bias, and can experience surface-induced rectification, which is used to build functional images of surface charge a surface. In the overwhelming majority of applications, however, SICM is used purely as a measure of local topography.

Generally, in SICM studies, the probe is distance-modulated, so that an alternating component of the ion current (AC) is induced at small tip-substrate separations. Another approach is to modulate the bias between QRCEs, which eliminates the need to physically perturb the probe position, termed bias modulation (BM)-SICM [62]. This reduces convection [63], electro-osmosis, and detrimental effects from extensive polarization of the QRCEs that could occur in distance-modulation SICM.

Differential-concentration (ΔC)-SICM, in which the electrolyte composition and concentration inside and outside the nanopipette is not identical, is particularly beneficial for live cell imaging since the electric field strength can be greatly diminished [64]. This technique also highlights the additional capability of an SICM probe for the delivery of molecules of interest to a surface (vide infra). This recent expansion of SICM into novel fields beyond topographical measurements has yet to be fully exploited, although it is a particularly well-suited technique for imaging living systems and single cells [6].

3.1. Combined SECM-SICM

The challenge to image chemical flux using SICM is addressed in different ways. One powerful way is to bring together the complementary techniques SICM and SECM, by making a probe with two-components, in combined SECM-SICM. Scanning ion conductance microscopy has traditionally been used to image topography, which also led to its use in combined techniques such as SECM-SICM, whereby chemical information is gathered using the SECM component of the probe, while the SICM component acts solely to measure topography. Originally, this was achieved using atomic layer deposition (ALD) of aluminum oxide to insulate a nanopipette coated with gold (on one side) [36], or similarly with a gold or Pt nanoring (Figure 1i) [37]. Focused ion beam (FIB) milling is a robust and reliable method to cut these nanotips, in order to give a planar electrode geometry [36,37]. A carbon ring/platinum disk electrode or carbon ring/nanopore electrode can be fabricated in which the electrode surfaces are also exposed using FIB milling [65]. FIB milling of carbon nanoelectrodes, prepared by chemical vapor deposition (CVD), has enabled high-resolution SECM imaging [50]. Pt nanotips may also be shaped using FIB, to achieve a lower insulating sheath radius for use with SECM [66].

More recently, the dual barrel pipette with pyrolyzed carbon in one of the two barrels (for the SECM component) has garnered interest due to the ease and speed of probe fabrication (Figure 1h) [67]. These double barrel carbon nanoprobes (DBCNPs), made using a quartz theta-pipette, can be used for localized chemical delivery, by filling the barrel used for SICM feedback with a molecule of interest. Nanopipette delivery in this form is affected by surface charge [68].

When SICM is coupled to SECM for investigation of cellular uptake, SICM can also be used to deliver species, loaded in the pipette barrel. For example, Unwin and coworkers [69] used a SECM-SICM probe to deliver hexaammineruthenium (III) ($[Ru(NH_3)_6]^{3+}$) to a *Zea mays* root hair cell (Figure 4). The $[Ru(NH_3)_6]^{3+}$ migrates out of the SICM barrel of the pipette, controlled by the applied potential to the electrode inside this barrel, and can be reduced at the SECM carbon electrode. Over an inert surface, the reduction current is higher than in bulk solution, due to the reduced diffusion field, whereas over a cell, there is a loss of ($[Ru(NH_3)_6]^{3+}$ into the cell via membrane transport (e.g., through ion channels), which results in an SECM current that is lower than in bulk solution.

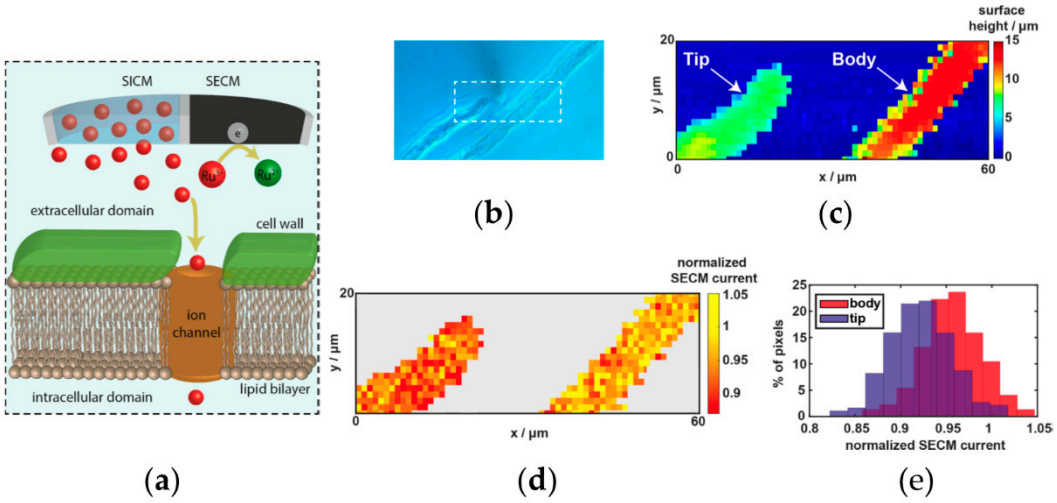

Figure 4. A dual barrel SECM-SICM probe is used to visualize molecular ($[Ru(NH_3)_6]^{3+}$) delivery and uptake at two regions of a single *Zea mays* root hair cell. (**a**) Schematic of the SECM-SICM setup, showing the probe positioned over a cell, in which $[Ru(NH_3)_6]^{3+}$ (Ru^{3+}) can diffuse/migrate from the delivering SICM barrel to the cell wall. Simultaneous measurement of ($[Ru(NH_3)_6]^{3+}$) reduction at the SECM electrode surface is made during the approach to the surface. This is compared to bulk (steady-state) current measurement for quantification. (**b**) Optical microscope image of the root hair cell. The dashed line marks the scanned area. (**c**) Topography image using the z-position at the end of each normal approach curve. (**d**) SECM current image over the sample, normalized to a bulk measurement at each pixel (current at the start of each normal approach curve). (**e**) Histogram plots of the normalized SECM current at each of the two regions of the root hair cell, labelled as "tip" and "body" in part (**c**). (Adapted with permission from Reference [69]. Copyright (2017) American Chemical Society).

3.2. *High-Resolution SECM-SICM*

The success of high-resolution electrochemical imaging using SEPM, with quantitative current measurements, depends on the design and geometry of the probe used. As the variety of probes used in SEPM platforms has increased, understanding the exact geometry has become increasingly important for quantitation of the current response [70]. Recently, comprehensive tip characterization of SICM probes has been explored using transmission electron microscopy (TEM) and ion conductance measurements, taking into account the effects of surface chemistry on the tip current response [55,70,71].

Another approach to improving tip geometry is the deposition of Pt on single barrel carbon probes (Figure 1b), which can be useful for the analytical detection of hydrogen peroxide [72]. Platinized carbon nanoelectrode probes possess very thin insulating sheaths, which are required for high-resolution SECM imaging [73], and deposition on recessed carbon electrodes offers additional control on the final tip geometry (recession depth) [9]. Pt-deposited carbon nanoelectrode SECM-SICM probes have been used to image hydrogen peroxide, exploiting the oxygen reduction reaction (ORR) on Pt [74].

Matsue and coworkers fabricated sphere-shaped Pt electrodes of different sizes, using highly controllable electrochemical deposition of Pt on the carbon-filled barrel of dual barrel SECM-SICM probes. Probes of increased sphere diameter are produced at increased current. This sphere-capped probe geometry led to electrodes with much improved sensitivity as compared to the bare carbon nanoelectrodes, due to enhanced faradaic current (Figure 5) [75]. It is also worth mentioning that these probes with protruding geometries maintain high resolution for imaging, yet have much improved sensitivity than a planar disk geometry, which should prove invaluable for using miniaturized biosensors for chemical imaging.

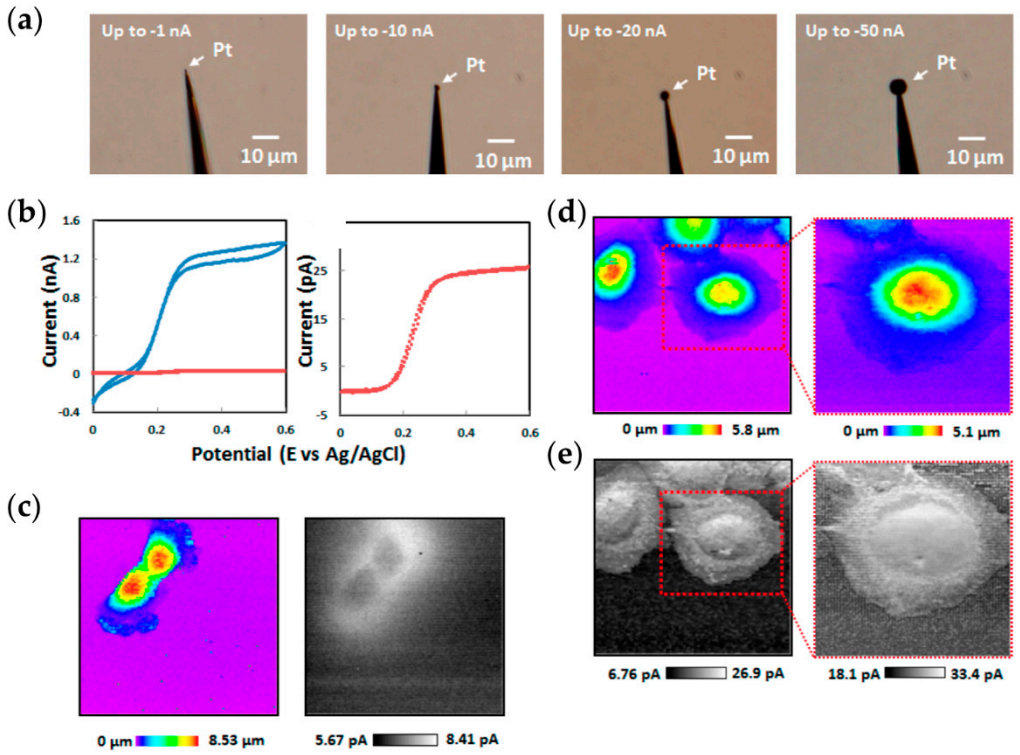

Figure 5. Dual barrel SECM-SICM probes are used to image immunocytochemically-stained EGFR proteins on A431 cells. (**a**) SECM-SICM probes with Pt sphere electrodeposited on the carbon SECM nanoelectrode, with increasing (left–right) amount of Pt deposition. (**b**) Cyclic voltammogram of a bare carbon nanoelectrode (red) and a Pt-deposited probe (blue) at −10 nA final deposition. (**c**) Topographic (left) and electrochemical (right) image of A431 cells acquired using a bare carbon electrode over an 80 × 80 µm scan area. (**d**) Topography and (**e**) electrochemical images of a A431 cells acquired using a Pt-deposited electrode, where the scan area is 75 × 75 µm on the left and 50 × 50 µm on the zoom-in (right). (Adapted with permission from Reference [75]. Copyright (2015) American Chemical Society).

4. Functional and Chemical Specific Probes for SECM

The development of electrochemical biosensors to quantitatively detect new targets has been a growing field that seeks to attain improvements in the fundamental analytical figures of merit, which include sensitivity, selectivity, limit of detection (LOD), and signal-to-noise ratio (SNR). As sensors become smaller, they may be implemented into an SEPM for chemical imaging, provided that the figures of merit are sufficient for an observable and meaningful measurement [76]. Pushing the spatial resolution of an imaging sensor can have a detrimental effect on other figures of analytical merit; in particular for the sensitivity of sensors predicated on surface-modified electrodes without the use of signal amplification.

Electrochemistry is a powerful tool in understanding neurotransmission, due to the spatial and temporal superiority over other techniques [77]. Carbon fiber electrodes are widely used to monitor neurotransmitters, catecholamines, and their metabolites, with a huge body of work focused on dopamine. Selectivity in the measurement arises from the unique redox potentials of the redox-active molecules of interest. This amperometric measurement may lack the selectivity to discriminate specific molecules with closely separated redox potentials, although fast scan cyclic voltammetry (FSCV) does allow better selectivity within a measurement. Interference from certain species can be minimized using chemical additives to the media, such as ascorbate oxidase to avoid the interference of ascorbic acid (present in extracellular media) [78]. However, methods of achieving better selectivity as well as addressing the need to detect non-electroactive species requires modified probes such as electrochemical biosensors.

An example of using a functional probe for imaging is the use of a dual electrochemical microsensor to simultaneously image oxygen and pH over the surface of a rat kidney [79]. The probe consisted of two recessed 10 μm diameter Pt electrodes, separated by 50–70 μm. One was modified with electrodeposited Pt followed by a coating of hydrophobic photocured polymer. This portion of the probe was used for amperometric detection of O_2, while the second was modified with an electrodeposited layer of iridium oxide (IrO_2) for pH mapping. The highly porous surface modification (Pt or IrO_2 layers) improved sensitivity and provided almost immediate response times of $t_{90\%}$ = 0.17 ± 0.005s for the O_2 sensor and $t_{90\%}$ = 0.43 ± 0.09s for the pH sensor. A similar approach has been used for dual barrel SECM-SICM probes that can function as a pH sensor, exploiting the pH sensitivity of IrO_2 [80].

4.1. Enzyme Modified Probes for Chemical Imaging in Scanning Electrochemical Microscopy

The enzyme activity of an enzyme-modified surface can be mapped using SECM [81], but electrode scanned probes modified with enzymes can themselves provide a means of achieving specific analyte recognition. Enzymes can be attached to the electrode surface directly, by covalent bonding, or by entrapment of the enzyme in a polymer film over the electrode surface. Immobilized enzyme sensors for species-selective have been implemented in the SECM [82], for example an enzymatic amperometric biosensor was used to measure the release of endogenous D-serine in the brain of stage 48 albino *Xenopus laevis* tadpoles [83]. This electrode had an appropriate dimension (25 μm diameter), and gave good temporal resolution to be used as a probe in SECM [84]. The probe itself consisted of a 25 μm diameter Pt disk electrode with an electrodeposited layer of ploy-*m*-phenylenediamine (PPD) and an adsorbed enzyme layer of D-amino acid oxidase from *Rhodotorula gracilis* (RgDAAO). Enzyme immobilization onto Pt UMEs by electropolymerization or casting was also performed to image single live cells using SECM, with electropolymerization leading to better spatial resolution of the probe, due to the smaller footprint of the enzyme modification [85].

The incorporation of biosensors on the micro- and nanoscales will find more use in SECM techniques, provided that achieving reproducible sensors with reasonable response times at the size-scale required for imaging is feasible. A drawback of enzyme-modified probes is that they typically respond slowly, which impedes the measurement of substrates that evolve rapidly. There are some examples of types of biosensors that could be used for chemical imaging that work using enzyme-modification [86]. An enzyme coating was deposited onto a 10 μm Pt UME, either by cross-linking, electropolymerization or adsorption, and was used for imaging glucose (mechanism shown in Figure 2a) and lactate (Figure 6) [87]. However, there remain challenges and opportunities in the miniaturization of enzyme-based sensors [88].

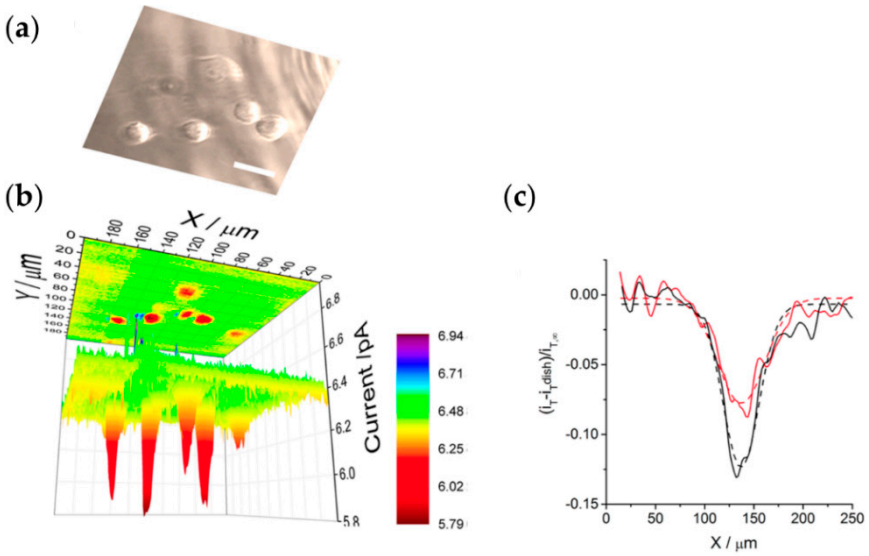

Figure 6. Imaging of glucose uptake by live cells using an enzyme-modified probe in SECM. (**a**) Optical microscope image of the scanned area covering several MCF10A cells. Scale bar is 30 µm. (**b**) Constant height SECM image of glucose uptake of the MCF10A cells, using electropolymerized 10 µm Pt GOx-UME biosensor. (**c**) Single line scans of the normalized current (to steady-state bulk current, $i_{T,\infty}$) of the biosensor probe over a single cell, where the measured tip current, i_T, is subtracted by the normalized currents on the Petri dish, i_{Tdish}. Black lines represent the convoluted activity and the topography contributions of the current and red lines represent only the topographical contribution. (Adapted with permission from Reference [87]. Copyright (2017) American Chemical Society).

4.2. Potential for Biosensor Probes in Scanning Electrochemical Microscopy

There are currently very few examples of scanning micro- or nanoscale biosensors for imaging applications. The key challenges are the miniaturization of the sensor, and implementing tip-positioning feedback. Noteworthy examples include carbon microelectrodes that have been modified with [NiFe]-hydrogenase embedded in a viologen-modified redox polymer hydrogel to produce a microbiosensor for hydrogen detection with high sensitivity (30 times higher current associated with hydrogen generation as compared with a bare Pt microelectrode) in scanning photoelectrochemical microscopy (SPECM) [89]. The real-time direct electrochemical detection of insulin was realized by the development of a miniaturized insulin sensor, by the incorporation of a multi-walled carbon nanotube (MWCNT)/dihydropyran film onto a 7 µm carbon fiber UME [90]. This sensor was used to measure insulin within extracellular media in the vicinity of a single pancreatic islet by performing a linescans over the islet, at different extracellular glucose concentrations.

In another class of biosensor, electrochemical aptamer-based (E-AB) sensors are a promising candidate for incorporation into electrochemical imaging probes for highly selective chemical imaging. Aptamers are short single-stranded DNA or RNA oligonucleotides or peptides that can be engineered to undergo reversible conformational changes when binding to a target molecule, with high specificity. E-AB sensors, which typically operate on the macroscale, can also be achieved on microelectrodes [91], at a size-scale that would allow for operation with SECM. Kelley and coworkers [92] produced nanostructured microelectrodes with diameters between 10 and 100 µm, which could be made into specific sensors for different bacterial targets by immobilization of a particular peptide nucleic acid (PNA) on the surface. As smaller biosensors become more widely used, applications in chemical imaging are expected to increase.

4.3. Scanning Ion-Selective Electrode Technique (SIET)

Small-scale ion-selective electrodes (ISEs) provide another means of achieving specific detection and imaging when coupled with SEPM. The ISEs may be glass membrane, solid state, liquid-based or compound electrodes. Ion-selective microelectrodes (ISMEs) operate on the size-scale that makes them useful for SECM and imaging. Bard and coworkers introduced scanning ISMEs (1 µm tip diameter) in 1995, selective for ions such as NH_4^+, K^+, and Zn^{2+}, and coupled with SICM for feedback [93]. Mg^{2+} ISMEs have been demonstrated for potentiometric SECM monitoring of Galvanic corrosion processes [94]. Carbon-based solid-state Ca^{2+} ISEs [95], and dual-electrode pH sensors with fast response times were used to quantitatively map the chemical environment at a model substrate bioactive glass (BAG) [95].

ISMEs are potentiometric probes with high impedance, which, in addition to the high capacitance of the measuring system, will result in long response times (i.e., several seconds). As a result, the imaging speeds attainable without image distortion will be limited [96]. Long scanning times are often a requirement for imaging using potentiometric SECM, which often means dynamically changing systems cannot be studied. Thus, there is great effort to reduce the response time of the ISME probe, as well as signal processing methods to deconvolute a raw distorted image obtained at high scan rate [97]. This type of correction, in which images can be obtained using systems that have not reached equilibrium at each pixel, can be obtained, at an order of magnitude faster than without the deconvolution. Temporal resolution is an important consideration for imaging, and especially so with potentiometric probes such as ISEs. Ions and anions must be measured slowly (0.5 to 1 s per pixel) due mainly to mechanical disturbance of the ion concentration gradient when the probe is moved but also to the time constant of the electrode, which is tenths of seconds for liquid ion exchanger (LIX) electrodes.

For improved spatial resolution, nano-ISEs have been prepared for imaging K^+ flux in living human embryonic kidney 293 cells (HEK293) (Figure 7) [98]. In this study, a 200–300 nm inner radius capillary was used, and each pixel in the image was the average of a 0.4 s interval measurement.

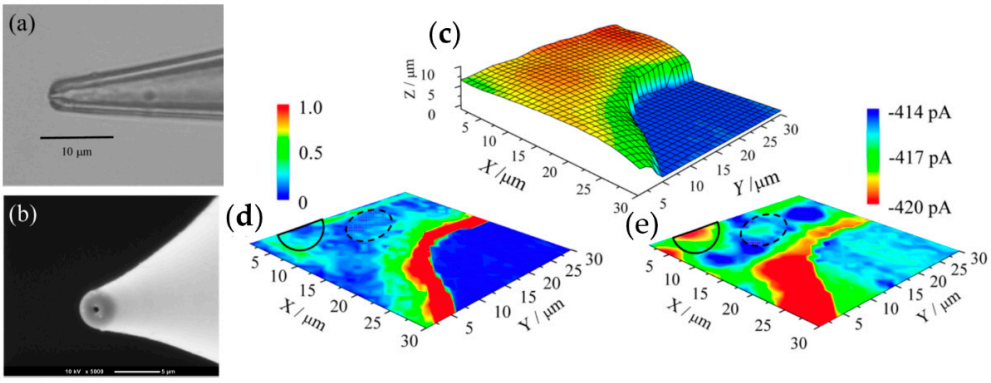

Figure 7. K^+-selective nanoelectrodes were used to simultaneously image topography and K^+ flux using SECM. (**a**) Optical microscopy image of a glass capillary used as an ion-selective nanoelectrode for SECM. (**b**) SEM micrograph of the same tip. (**c**) Topography image. (**d**) Maximum gradient of the sample surface image. (**e**) SECM current image of HEK293 cells. (Adapted with permission from Reference [98]. Copyright (2014) American Chemical Society).

5. Biosensor Probes in Scanning Ion Conductance Microscopy

5.1. Functionalized Glass Nanopipettes for Ion Gating Based Sensors

Nanopipettes can be functionalized, typically with a protein that binds to a specific target and undergo a signal change to function as a sensor, which has been termed signal transduction by ion nanogating (STING) (e.g., Figure 2d). There are a few examples of nanopipettes modified with proteins

to produce reversible sensors that respond to a specific target molecule. For example, glucose oxidase has been surface immobilized on the inner walls of a glass nanopipette to function as a glucose sensor, used for intracellular detection of elevated glucose levels in single cancer cells [99]. Also, a glass nanopipette was functionalized with calmodulin protein which reversibly binds to cations such as Ca^{2+}, resulting in a decrease in current at a negatively biased pore [100]. While a large area of the glass nanopipette is functionalized with an antibody, DNA, peptide or aptamer, due to a high impedance of nanopipettes, the sensitivity of the device is confined to within a micron of the 50 nm tip orifice. These probes offer the size-scale and fast response times required for SEPM imaging, but functional mapping at the nanoscale has yet to be realized in this emerging field. Nanopipettes functionalized with specific recognition elements are a promising developing area of research that could yield biosensors capable of imaging at the single cell level [101]. In particular, aptamer-functionalized nanopipettes demonstrate reversible response to a target, not readily observed with antibody-modified nanopipettes [102]. Pourmand and coworkers [103] used the ion current through an aptamer functionalized STING sensor nanopipette to demonstrate reversible and quantitative detection of thrombin. This technology has been limited to bulk solution measurements thus far, but imaging using the principles of STING should be practically achievable, since these sensors can be readily and cheaply made at nanometer dimensions (typically 100 nm diameter at the tip orifice) and they demonstrate reversibility to changing target concentration, with a response time of a few seconds (faster response times may be expected with smaller target molecules).

5.2. Ion Channel Probe-Based Scanning Ion Conductance Microscopy

A particularly exciting and emerging recent development in the field of SICM is the use of a probe that supports a lipid bilayer at the tip, into which ion channels are embedded, thus providing specificity and very high signal to noise ratios. Ion channels are nature's nanopores that can be exploited as nanoscale biosensors by monitoring changes in an ion current that flows through the channel(s) [104]. Different membrane proteins that bind to specific targets, including previously unattainable molecules, can be incorporated into a lipid bilayer to enable molecule-specific nanoscale biosensors with single molecule sensitivity.

A lipid bilayer can be formed at the end of a glass micropipette [105,106], which can then be employed in a scanning probe microscope, such as a scanning ion conductance microscope (SICM) [57]. Combining an ion channel probe with SICM allows for localized quantitative concentration mapping of a target analyte. Recently, ion channel-based probes (ICPs) for SICM have been introduced, which can operate either using a single barrel (Figure 2e) [107,108] or a dual barrel pipette (Figure 2f) [109]. The dual barrel approach offers the potential advantages of decoupling the SICM feedback current and ICP current measurements, and allowing operation with fewer ion channels which may sometimes be beneficial. These approaches allow topography imaging [107], as well as simultaneous topography and selective molecular flux mapping [108,109]. These ICPs for SICM provide a means to quantitatively elucidate mechanistic and spatial information on important biological transport processes.

An alpha-hemolysin (αHL) ion channel was incorporated into a lipid bilayer at the opening of a glass micropore pipette, and was used to image β-cyclodextrin (βCD) and heptakis(6-*O*-sulfo)-β-cyclodextrin (S_7βCD) diffusing out of a glass micropore substrate (Figure 8) [108]. These cyclodextrin molecules can enter and exit the β-barrel region of the αHL protein, causing a transient blocking of ion current through the pore. As a proof-of-concept, the imaging spatial resolution was fairly poor, although this was partially due to the requirement to spend a sufficient amount of time at each pixel (30 s) in order to collect enough events for some qualitative (if not quantitative [110]) analysis of ligand concentration by capturing channel-blocking events in the current-time signal. The αHL ion channel is very widely studied [111], but does not have the ability to bind to specific molecules of interest, and thus lacks practical application as a biosensor.

Baker and coworkers [109] used human embryonic kidney293 cells transfected with Big Potassium (BK) channels (i.e., large-conductance, voltage, and calcium-activated potassium channels) onto which

patch clamp measurements could be made. Using suction, membrane patches could be extracted from single cells, and probes were made in both the outside-out and inside-out configurations. Using a double barrel probe for membrane-patching required the pipettes to be fire-polished to minimize capacitative artifacts and facilitate a gigaseal membrane across the opening [109]. This method of membrane patching opens up the range of ion channels that can be incorporated into a ICP [109,112]. The library of proteins that has been exploited for use in nanopore-based biosensors is still small. More challenging proteins, such as heat shock cognate 70 (Hsc70), which forms a multi-conductance state pore in the presence of adenosine triphosphate (ATP), can also be incorporated into a lipid bilayer. For this non-well behaved channel, the charge flux has been monitored as a means to quantify ATP concentration from the current-time response [113].

There are significant challenges that make chemical imaging using ion channel nanopores difficult to implement. It is highly conceivable that the use of specific ligand-gated ion channels will find further use with complementary techniques such as SICM for imaging, where the SICM component of the probe functions for topography mapping of a substrate, and the ion channel component of the probe functions to give quantitative chemical information at particular locations of a sample. Various attempts at quantifying ion channel activity to specific species concentration, including for multiple channels [110], have been demonstrated [112,113]. Dual barrel ICPs are thus required to decouple the distance feedback from the ion channel activation so that quantitative chemical imaging can be realized.

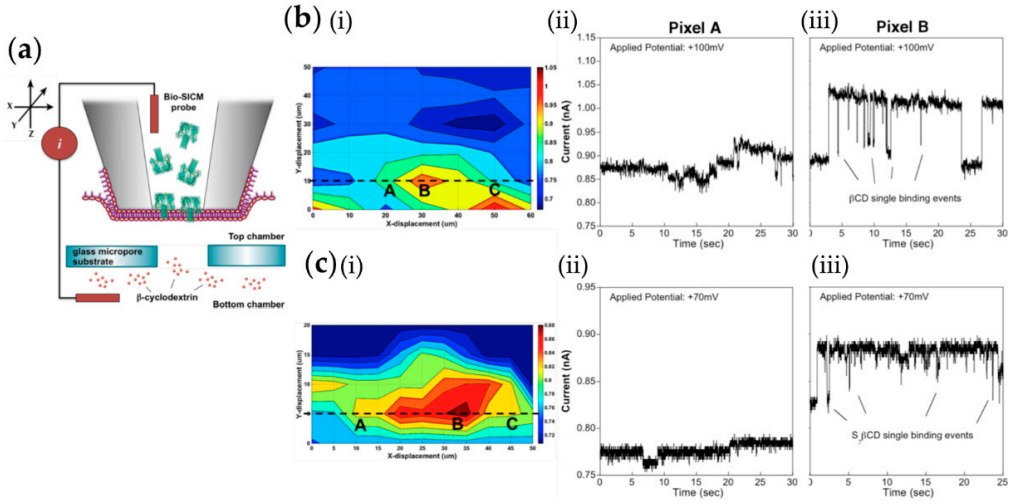

Figure 8. Single barrel ion channel probes can be used to image a substrate. (**a**) Schematic of the single barrel ion channel-based probe (ICP) SICM set up, showing a probe above a glass micropore containing 100 mM of βCD. (**b**) (i) Average current image shows the effect of changing topography, with highest current directly over the pore. Current-time traces of the ICP barrel obtained at (ii) pixel A, over the glass substrate and (iii) pixel B, directly over the micropore where the observed binding event frequency is highest. (**c**) Same as (**b**), except S_7βCD was used in the pore instead. (Adapted with permission from Reference [108] (https://pubs.acs.org/doi/abs/10.1021/jacs.5b13252). Copyright (2016) American Chemical Society. Further permissions related to the material excerpted should be directed to the ACS).

6. Advanced Scanning Modes of SEPM Including Fast Scanning and Imaging Movies

6.1. Hopping Imaging Modes of SICM and SECM

A hopping mode of scanning was conceived as a means to probe topographically challenging substrates [114], since the probe performs a short approach curve at every pixel in the image. This minimizes the time the probe spends close to the substrate, but is also advantageous in that current information can be collected during the approach and plotted to give chemical

concentration information away from as well as at the surface, as in hopping intermittent contact (HIC)-SECM [115]. This was first demonstrated using four-dimensional shear-force-based constant-distance (4D SF/CD)-SECM, in which shear-forces were used to obtain sample topography and images were collected at a series of (constant) distances from the surface [116]. The same approach has been termed depth scan mode for imaging topography of cells [117] and tracking live cell response to Cd^{2+} concentrations [118,119].

Collecting a measurement at the surface, and a second measurement in bulk solution (i.e., far enough away from the surface that any surface feedback effects have little to no effect on the measurement), allows self-referencing of the probe. At each pixel in the image, the probe is calibrated, so that changes in probe response over time can be accounted for, which is especially important for lengthy experiments or measurements performed in living systems that may be more dynamic and change over time [69].

6.2. Fast Scanning and Imaging Movies Obtained with SEPM

Mauzeroll and coworkers [120], used probe speeds in SECM of 50 $\mu m \cdot s^{-1}$ to scan linescans of a single HeLa cell. For SECM, the challenge of high-speed imaging remains the availability of models that take into account the effects of increased and forced convection, fluid flow and changes to diffusion, caused by the probe moving at increased velocities [120–122].

Typical hopping scans withdraw the tip after every approach to the surface by a constant height, which negatively affects temporal resolution. Matsue and coworkers [123] used a new scanning algorithm to perform hopping SICM at high speeds, through which the amplitude of the tip withdrawal was controlled. Briefly, very short approaches were used, which could result in a contact between tip and sample. If this happens, the tip could be withdrawn a few steps (in the x-direction) and approaches with a greater withdrawal amplitude can be used for that region of more challenging topography on the surface. Since smoother regions can be scanned faster, a topography image was collected every 18 s (64 × 64 pixels at 10 × 10 μm for an image of microvilli on an A431 cell). There are other examples of creative scanning modes such as using algorithms to correct for image skew that could be a problem with potentiometric SEPM at fast scan rates, provided the object being imaged is symmetrical [124], and using the predicted movement of a pipette during imaging over parts of a sample that the topography does not change much [125].

Another recent theme in electrochemical imaging has been producing quantitative movies of activity of a sample. Each frame in a movie can correspond to a potential in a voltammogram, obtained by performing linear sweep voltammetry (LSV) or cyclic voltammetry (CV) at every pixel in the scan (position on the substrate). The frames can be made from repetitive scans over an area of interest, where each frame of the movie is a new scan of the surface, which may change over time. Alternatively, the frames can be made by performing dynamic voltammetric measurements at each pixel in a single scan, such as linear sweep voltammetry (LSV) or cyclic voltammetry (CV), to construct a movie in which each frame corresponds to a different potential.

Originally conceived as a dual barrel pipette based technique (Figure 2g) [126], and most recently in a single barrel format (Figure 2h) [127], scanning electrochemical cell microscopy (SECCM) is a droplet cell-based imaging technique. The advantages of a droplet electrochemical cell are that the contact area of the meniscus defines the area of the substrate that is probed at each pixel. This is in contrast to techniques like SECM and SICM, in which the entire surface needs bathing in solution. This does limit the technique to non-biological samples, since cells require a stable solution-based environment for healthy and proper function. Movies of electrochemical activity have been performed using LSV-SECCM for the hydrogen evolution reaction (HER) on MoS_2 to study the intrinsic activity of the edge and basal plane sites [127,128]. Unwin and coworkers [129] have implemented a non-raster-scan pattern following a spiral trajectory for faster imaging with SECCM. Image sequences were collected with a frame rate of 0.24 fps, meaning an image was recorded every 4 s. This is orders of magnitude higher than has been achieved before. The droplet probe had a radius

of 200 nm, giving high spatial resolution too, with about 1000 pixels·um^{-2}. Images were able to be made at 4 s per frame due to the high data recording rate, fast probe response and piezo stages that have low capacity and high resonance frequency. The SECCM technique is incapable of performing measurements on cells that require continuous bathing in an extracellular fluid, but it represents a key direction in SEPM technology for the faster scanning of substrates at high resolution. Fast scanning with SICM has been applied to noninvasive imaging of microvilli on cell surfaces, with images taken every 18 s and used to measure the movement speeds of different shapes of microvilli [123]. There remains scope for integration of fast scanning protocols with SECM, using appropriate distance feedback such as ion conductance in combined SECM-SICM, which would allow imaging of a much wider range of samples that include cells. To take advantage of the fast scan capability, processes occurring over the timescale of few seconds to minutes should be studied.

In the last five years, advances in the scanning pattern and fast response of tip-positioning has facilitated imaging with frame rates up to 0.24 fps. In these examples, both high spatial and high temporal resolution are achieved. There are alternative strategies to increase the temporal resolution of electrochemical imaging, such as by using microelectrode arrays.

7. Microelectrode Arrays and Large-Scale Integration Chips

Electrochemical imaging can also be achieved without the use of a scanned probe, through the use of an individually addressable microelectrode array (MEA) or similar devices. Microelectrode arrays have been presented as a means to "image" single cells, rapidly and quantitatively [130,131]. Ewing and coworkers [131] used well-based MEAs, with 16 × 4 μm, 25 × 3 μm, or 36 × 2 μm square ultramicroelectrodes at a few microns separation, each in a 40 × 40 μm area dimensions that allowed for examining exocytosis events from a single pheochromocytoma PC12 cell. Video imaging data were presented at 8-electrodes that the cell covered, showing subcellular spatial heterogeneity of exocytotic release. The devices were coated in a mouse collagen IV solution that promoted adhesion of the PC12 cells, so they could grow directly over the electrode wells of the MEA. Subsequent work was carried out that deployed a movable lithographically fabricated thin film MEA, to perform two-dimensional imaging of single vesicle release events [132], obtaining a balance between spatial resolution (1.2 μm closely packed electrodes) and very good temporal resolution. This method relied on there being enough molecules in a single exocytosis event that they could be detected by three or more opposing electrodes, by modelling the response at these electrodes to locate the origin of exocytotic release. This was employed to distinguish heterogeneity within a single chromaffin cell surface for the release of catecholamine, stimulated by $BaCl_2$ and $MgCl_2$.

Large-scale integration (LSI) chips, which pair a charge-coupled device (CCD) and a complementary metal-oxide semiconductor (CMOS) sensor, have been used to image biomolecule concentrations typically on a millimeter scale with pixels (sensors) 10s of μm across. This is a much larger scale than is generally used for SEPM imaging, bar a few exceptions [133]. This type of sensor is useful for high-throughput analysis, largely because it offers the ability to probe many samples at once, under well-defined conditions. As an imaging tool, the size of the device, and inherently needed electrode separation distance, will limit its use. Due to the limitations of device size and structure, this type of imaging will typically have lower resolution [134]. Matsue and coworkers [135] used an amperometric sensor array device at a size-scale suited to cell clusters.

Matsue and coworkers [135] have been instrumental in developing this type of imaging platform, with the most widely used application being interrogation of 3D cultured cells using electrochemical chip devices. Microelectrode arrays require time-consuming and sophisticated fabrication methods. Also, the interelectrode spacing is an important factor that governs spatial resolution, since electrodes need to be sufficiently separated to avoid chemical cross-talk between adjacent electrodes. To enhance the ability of the sensor array device, the approach has been extended to offer simultaneous multi-reaction imaging. In electrochemicolor imaging, two (or more) different potentials are applied at alternate electrodes within the array (Figure 9) [136]. Alternate potentials can be applied at alternate

electrodes on the device (V1 and V2 modes in Figure 9), with only moderate loss of imaging spatial resolution, using a mathematical approach to fill in the now "missing" pixels. Importantly, current is measured simultaneously at all pixels, so temporal resolution is not affected. This is demonstrated for the simultaneous imaging of activities of glucose oxidase (GOx) and alkaline phosphatase (ALP) at enzyme membranes (Figure 9) as a proof of principle, and for mouse ES cell cultures (embryoid bodies). The enzymatic reaction of glucose oxidase (GOx) with glucose consumes O_2, leading to a lower measured current associated with O_2 reduction at the electrode surface, which was held at a potential of −0.5 V. Similarly, alkaline phosphatase (ALP) reacts with *p*-aminophenol phosphate (PAPP) to form *p*-aminophenol (PAP), which was measured electrochemically at the electrode surface by oxidation to *p*-quinone imine (QI). These indirect measurements of non-electrochemically active species are common for biosensor platforms, and the ability to hold different potentials for different electrodes within an array partly overcomes the problem of selectivity, since it is possible to monitor multiple biomolecules simultaneously. Furthermore, images acquired using this platform show the activities associated with two molecules, using two color scales to differentiate between the electrode potential at which the current was collected.

Another novel approach is integrating a MEA and microfluidic device for chemical imaging using electrochemistry. Scanning electrochemical probe microscopy is incompatible with closed microchannels, due to the requirement of a scanned probe positioned directly above the substrate. The first imaging using in situ voltammetry for microfluidics used a 20 × 10 electrode array (Figure 10) [137]. This technique has inherently very low spatial resolution, which could be as low as 25 µm for 340 × 340 µm electrodes, limited by the device fabrication. While this technique suffers poor spatial resolution as compared with SEPM, very fast temporal resolution is achieved. Moreover, this type of device further illustrates the possibility of chemical imaging in environments that SEPM is not feasible.

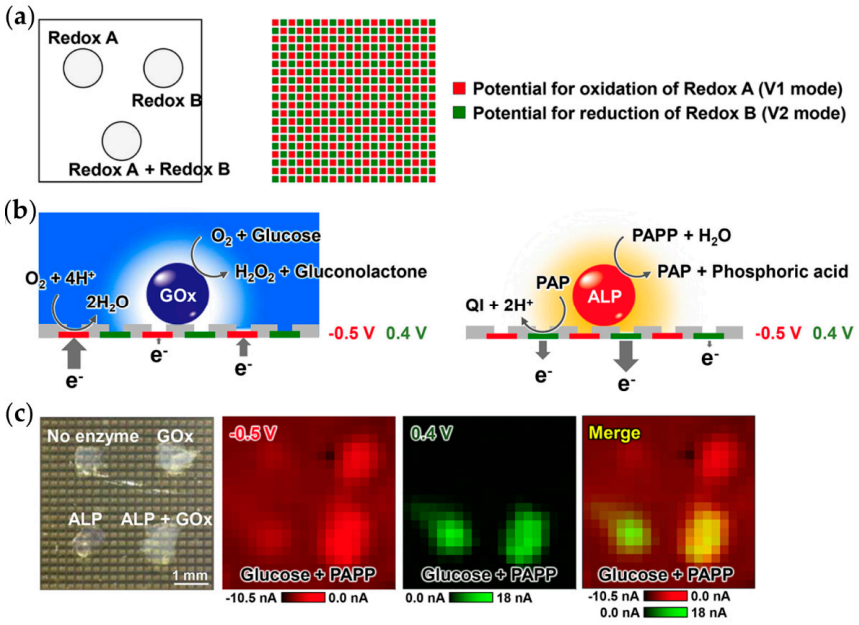

Figure 9. Principles and example images using electrochemicolor imaging. (**a**) Schematic of a sample over a microelectrode array that has individual alternate electrodes set at a potential to oxidize redox species A (red) and reduce redox species B (green). (**b**) Schematics for the detection mechanism of GOx activity (left) and ALP activity (right). (**c**) Optical microscope image (left) and electrochemical current images (right three panels) of four membranes on the microelectrode array (MEA) device with glucose and PAPP. (Adapted with permission from Reference [136] (http://pubs.acs.org/doi/10.1021/acs.analchem.7b03042). Further permissions related to the material excerpted should be directed to the ACS).

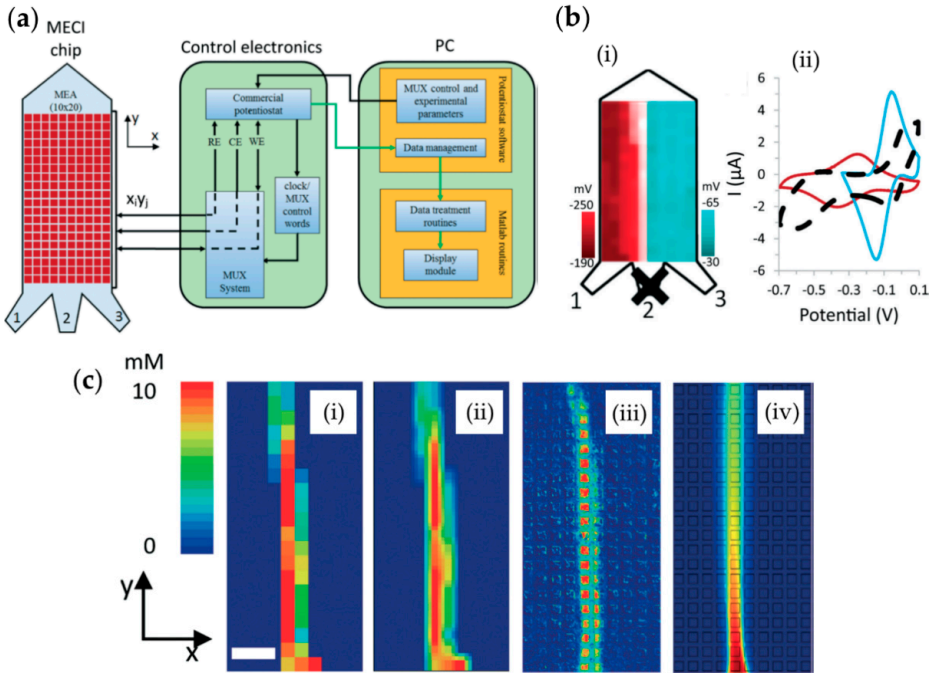

Figure 10. Electrochemical imaging for microfluidics on a microfluidic electrochemical imaging (MECI) chip. (**a**) Schematic of microfluidic device housing a MEA, where RE is the reference electrode, CE is the counter electrode, WE is the working electrode, and MUX is a low-noise multiplexer. (**b**) (i) Electrochemical image of a co-flow of $Ru(NH_3)_6^{3+}$ (red) and $Fe(CN)_6^{3-}$ (blue) at inlet 1 and 3, respectively. (ii) Representative CVs for $Ru(NH_3)_6^{3+}$ (red), $Fe(CN)_6^{3-}$ (blue), and the overlapping region (black dashed), without baseline correction. (**c**) Electrochemical image of 10 mM $Fe(CN)_6^{3-}$ stream from inlet 2, with confinement streams from inlets 1 and 3. (i) Raw data, (ii) after smoothing algorithm applied (iii) optical image with dye added to the analyte and (iv) computer simulation. Scale bar is 1 mm. (Adapted from Reference [137] with permission of The Royal Society of Chemistry).

Using 64 subarrays of 128 individual Pt working electrodes, high-density MEAs of 8192 individually addressable electrodes were created and used to map norepinephrine across a 2 × 2 mm area [138]. Temporal resolution was limited to 10 ms per subarray, or 64 s at a rate of 1 Hz per subarray. Spatial resolution was limited to 30 μm. As pointed out in their work, this system should be best suited to augment traditional microscopy methods and as a tool to image chemical distributions in biological systems. In a proof-of-concept design proposed by Henry and coworkers [139], using only four devices (each with a 130 μm sampling port leading to carbon paste electrodes (CPEs)), the chemical gradient of dopamine was probed across a 3 mm length scale (sampling ports positioned 1 mm apart)) over hundreds of seconds (with continuous measurement of current). While this may not strictly be considered imaging (currents were only spatially resolved in one-dimension), the results serve well as an introduction to the benefits of using multiple electrode platforms for the spatiotemporal resolution of targets that do not require the use of fluorescent or chemiluminescent active targets as used in other microscopy platforms.

Scanning electrochemical probe microscopy is limited to in vitro systems; however, a promising method in the application of biosensor probes to realize a real-time spatially resolved imaging strategy in vivo is to use devices with a low-number of (multiple) electrodes over a large area [140]. As a particularly useful method for spatially resolved measurements in challenging biological systems, such as intracortical recordings, this technology is still developing [141]. It has been shown that flexible neural probes can be inserted into living tissue, with the assistance of a stiffener assembly, in a further example of an application of electrochemical imaging in a location inaccessible to standard SEPM methods operated with a mobile scanning probe [142]. Although this concept has yet to be

applied to producing images of chemical concentration, different sensors for multi-analyte detection (e.g., glutamate and dopamine) or for spatially resolved measurements has been achieved [143].

The first report of an application of a LSI-based device for real-time electrochemical-based long time (over 3 h) monitoring of cells, was demonstrated for measuring alkaline phosphatase (ALP) from embryoid bodies [144]. Other devices have been made that are suitable for large substrate surfaces that require rapid electrochemical imaging. Topography and conductivity were measured using a LSI-based device with 400-electrode sensors to produce images of a series of large substrate surfaces [145]. Potentiometric bioimaging using the same LSI-based device was achieved by modifying the electrodes for enzyme activity measurements of glucose oxidase and ALP, at embryonic stem (ES) cells [146]. Microelectrode arrays are amenable to biosensor modifications, and these devices represent a promising new tool for bioimaging of enzyme activity and chemical concentrations over large areas (mm scale). An important consideration for achieving higher resolution imaging when using MEAs is the possibility of cross-talk between adjacent electrodes, although this can be avoided if the thickness of the diffusion layer of each microelectrode is less than half the separation distance between the electrodes.

Lindau and coworkers showed that single vesicle release events from chromaffin cells were resolved from spikes in the current-time traces (which constituted the pixels of the electrochemical image) owing to the low pA current resolution and effective temporal resolution of 0.5 ms (giving a sensitivity of ~6000 molecules) [147]. The device comprised a 100-electrode array (10 $\times$ 10 low noise complementary metal–oxide–semiconductor (CMOS) potentiostat array) that was used to detect dopamine release.

8. Conclusions and Perspectives

In this review, the recent advances in chemical imaging using electrochemical methods have been summarized, with a particular focus on scanning methods that use principles of SECM and SICM for cell imaging. There has been much attention on the improvements in both spatial and temporal resolution in electrochemical imaging. With spatial resolution, smaller probes used in SEPM offer improved resolution, provided that the chemical sensing ability of electrodes at low micro- and nanoscale sizes matches those of their macroscale equivalents. With temporal resolution, improvements in SEPM have required piezoelectric positioners with a high-resonance frequency.

The alternative to SEPM is to use MEA devices, although there are technical challenges that limit the spatial resolution of these platforms. MEAs have the advantage with temporal resolution given that scanned probes (with the exception of soft linear array probes) cannot take numerous concurrent measurements at different locations of a sample. MEA devices can't readily image topography, and the type of sample studied should be considered using the spatial resolution limits. MEA devices will be most useful for high throughput analysis, and could prove valuable as a new tool to study organ-on-a-chip systems, due to the ability to integrate microfluidics into the device.

A future direction of electrochemical imaging will be the further integration of complementary techniques, as has been successfully achieved for SECM-AFM, SECM-SICM and most recently ICP-SICM. The integration of biosensors that offer specificity for a target of interest to SEPM is particularly exciting, since non-electrochemically active molecules may be detected using sensors with high specificity. There are further opportunities to couple electrochemical imaging platforms with other techniques, such as SECM-ATR and SECM-Raman.

Scanning ion conductance microscopy in the traditional sense does not provide chemical information, but it is a powerful tool in SEPM as a means of topography determination, and has proven useful for local delivery of molecules to a substrate. SECM offers chemical imaging, especially in solutions of few interfering species, although selectivity is usually limited to redox-active molecules that can be distinguished by their sufficiently unique redox potentials. Electrochemical biosensors, ion-selective electrodes and ion channel probes offer superior selectivity, though these types of probes require additional time and care in fabrication. The field of electrochemical biosensors has thus

far largely presented opportunities for point-of-care applications that employ macroscale sensors. Further applications of miniaturized sensors used in SEPM can be expected within the emerging fields of quantitative measurement of specific targets using ICPs and STING sensors for SICM and E-AB sensors for SECM.

Acknowledgments: This material is based upon work supported by the National Science Foundation under CHE-1608679.

Conflicts of Interest: The authors declare no conflict of interest.

References

1. Li, Y.; Ning, X.; Ma, Q.; Qin, D.; Lu, X. Recent advances in electrochemistry by scanning electrochemical microscopy. *TrAC Trends Anal. Chem.* **2016**, *80*, 242–254. [CrossRef]
2. Zoski, C.G. Review—Advances in Scanning Electrochemical Microscopy (SECM). *J. Electrochem. Soc.* **2016**, *163*, H3088–H3100. [CrossRef]
3. Izquierdo, J.; Knittel, P.; Kranz, C. Scanning electrochemical microscopy: An analytical perspective. *Anal. Bioanal. Chem.* **2018**, *410*, 307–324. [CrossRef] [PubMed]
4. Bergner, S.; Vatsyayan, P.; Matysik, F.-M. Recent advances in high resolution scanning electrochemical microscopy of living cells—A review. *Anal. Chim. Acta* **2013**, *775*, 1–13. [CrossRef] [PubMed]
5. Schulte, A.; Nebel, M.; Schuhmann, W. Scanning Electrochemical Microscopy in Neuroscience. *Annu. Rev. Anal. Chem.* **2010**, *3*, 299–318. [CrossRef] [PubMed]
6. Page, A.; Perry, D.; Unwin, P.R. Multifunctional scanning ion conductance microscopy. *Proc. R. Soc. Lond. Ser. A* **2017**, *473*, 20160889. [CrossRef] [PubMed]
7. Takahashi, Y.; Kumatani, A.; Shiku, H.; Matsue, T. Scanning Probe Microscopy for Nanoscale Electrochemical Imaging. *Anal. Chem.* **2017**, *89*, 342–357. [CrossRef] [PubMed]
8. Kranz, C. Recent advancements in nanoelectrodes and nanopipettes used in combined scanning electrochemical microscopy techniques. *Analyst* **2014**, *139*, 336–352. [CrossRef] [PubMed]
9. Kang, M.; Momotenko, D.; Page, A.; Perry, D.; Unwin, P.R. Frontiers in Nanoscale Electrochemical Imaging: Faster, Multifunctional, and Ultrasensitive. *Langmuir* **2016**, *32*, 7993–8008. [CrossRef] [PubMed]
10. Kueng, A.; Kranz, C.; Mizaikoff, B. Scanning Probe Microscopy with Integrated Biosensors. *Sens. Lett.* **2003**, *1*, 2–15. [CrossRef]
11. Bard, A.J.; Fan, F.R.F.; Kwak, J.; Lev, O. Scanning electrochemical microscopy. Introduction and principles. *Anal. Chem.* **1989**, *61*, 132–138. [CrossRef]
12. Engstrom, R.C.; Pharr, C.M. Scanning Electrochemical Microscopy. *Anal. Chem.* **1989**, *61*, 1099–1104. [CrossRef]
13. Bard, A.J.; Fan, F.-R.F.; Pierce, D.T.; Unwin, P.R.; Wipf, D.O.; Zhou, F. Chemical Imaging of Surfaces with the Scanning Electrochemical Microscope. *Science* **1991**, *254*, 68–74. [CrossRef] [PubMed]
14. Payne, N.A.; Stephens, L.I.; Mauzeroll, J. The Application of Scanning Electrochemical Microscopy to Corrosion Research. *Corrosion* **2017**, *73*, 759–780. [CrossRef]
15. Perry, A.R.; Lazenby, R.A.; Adobes-Vidal, M.; Peruffo, M.; McKelvey, K.; Snowden, M.E.; Unwin, P.R. Hopping intermittent contact-scanning electrochemical microscopy (HIC-SECM) as a new local dissolution kinetic probe: Application to salicylic acid dissolution in aqueous solution. *CrystEngComm* **2015**, *17*, 7835–7843. [CrossRef]
16. Ishimatsu, R.; Kim, J.; Jing, P.; Striemer, C.C.; Fang, D.Z.; Fauchet, P.M.; McGrath, J.L.; Amemiya, S. Ion-Selective Permeability of an Ultrathin Nanoporous Silicon Membrane as Probed by Scanning Electrochemical Microscopy Using Micropipet-Supported ITIES Tips. *Anal. Chem.* **2010**, *82*, 7127–7134. [CrossRef] [PubMed]
17. Oyamatsu, D.; Hirano, Y.; Kanaya, N.; Mase, Y.; Nishizawa, M.; Matsue, T. Imaging of enzyme activity by scanning electrochemical microscope equipped with a feedback control for substrate-probe distance. *Bioelectrochemistry* **2003**, *60*, 115–121. [CrossRef]
18. Gyurcsányi, R.E.; Jágerszki, G.; Kiss, G.; Tóth, K. Chemical imaging of biological systems with the scanning electrochemical microscope. *Bioelectrochemistry* **2004**, *63*, 207–215. [CrossRef] [PubMed]

19. Heinze, J. Ultramicroelectrodes in Electrochemistry. *Angew. Chem Int. Ed. Engl.* **1993**, *32*, 1268–1288. [CrossRef]
20. Kwak, J.; Bard, A.J. Scanning electrochemical microscopy. Theory of the feedback mode. *Anal. Chem.* **1989**, *61*, 1221–1227. [CrossRef]
21. Martin, R.; Unwin, P. Scanning electrochemical microscopy Kinetics of chemical reactions following electron-transfer measured with the substrate-generation-tip-collection mode. *J. Chem. Soc. Faraday Trans.* **1998**, *94*, 753–759. [CrossRef]
22. Eckhard, K.; Chen, X.; Turcu, F.; Schuhmann, W. Redox competition mode of scanning electrochemical microscopy (RC-SECM) for visualisation of local catalytic activity. *Phys. Chem. Chem. Phys.* **2006**, *8*, 5359–5365. [CrossRef] [PubMed]
23. Rodríguez-López, J.; Alpuche-Avilés, M.A.; Bard, A.J. Interrogation of Surfaces for the Quantification of Adsorbed Species on Electrodes: Oxygen on Gold and Platinum in Neutral Media. *J. Am. Chem. Soc.* **2008**, *130*, 16985–16995. [CrossRef] [PubMed]
24. Wuu, Y.; Fan, F.F.; Bard, A.J. High Resolution Deposition of Polyaniline on Pt with the Scanning Electrochemical Microscope. *J. Electrochem. Soc.* **1989**, *136*, 885–886. [CrossRef]
25. Denuault, G.; Frank, M.H.T.; Peter, L.M. Scanning electrochemical microscopy: Potentiometric probing of ion fluxes. *Faraday Discuss.* **1992**, *94*, 23–35. [CrossRef]
26. Díaz-Ballote, L.; Alpuche-Aviles, M.; Wipf, D.O. Fast-scan cyclic voltammetry–scanning electrochemical microscopy. *J. Electroanal. Chem.* **2007**, *604*, 17–25. [CrossRef]
27. O'Connell, M.A.; Wain, A.J. Combined electrochemical-topographical imaging: A critical review. *Anal. Methods* **2015**, *7*, 6983–6999. [CrossRef]
28. Eckhard, K.; Schuhmann, W. Alternating current techniques in scanning electrochemical microscopy (AC-SECM). *Analyst* **2008**, *133*, 1486–1497. [CrossRef] [PubMed]
29. Wipf, D.O.; Bard, A.J. Scanning electrochemical microscopy. 15. Improvements in imaging via tip-position modulation and lock-in detection. *Anal. Chem.* **1992**, *64*, 1362–1367. [CrossRef]
30. Hengstenberg, A.; Kranz, C.; Schuhmann, W. Facilitated Tip-Positioning and Applications of Non-Electrode Tips in Scanning Electrochemical Microscopy Using a Shear Force Based Constant-Distance Mode. *Chem. A Eur. J.* **2000**, *6*, 1547–1554. [CrossRef]
31. McKelvey, K.; Edwards, M.A.; Unwin, P.R. Intermittent Contact-Scanning Electrochemical Microscopy (IC-SECM): A New Approach for Tip Positioning and Simultaneous Imaging of Interfacial Topography and Activity. *Anal. Chem.* **2010**, *82*, 6334–6337. [CrossRef] [PubMed]
32. Sundaresan, V.; Marchuk, K.; Yu, Y.; Titus, E.J.; Wilson, A.J.; Armstrong, C.M.; Zhang, B.; Willets, K.A. Visualizing and Calculating Tip–Substrate Distance in Nanoscale Scanning Electrochemical Microscopy Using 3-Dimensional Super-Resolution Optical Imaging. *Anal. Chem.* **2017**, *89*, 922–928. [CrossRef] [PubMed]
33. Edwards, M.A.; Whitworth, A.L.; Unwin, P.R. Quantitative Analysis and Application of Tip Position Modulation-Scanning Electrochemical Microscopy. *Anal. Chem.* **2011**, *83*, 1977–1984. [CrossRef] [PubMed]
34. Ludwig, M.; Kranz, C.; Schuhmann, W.; Gaub, H.E. Topography feedback mechanism for the scanning electrochemical microscope based on hydrodynamic forces between tip and sample. *Rev. Sci. Instrum.* **1995**, *66*, 2857–2860. [CrossRef]
35. Ballesteros Katemann, B.; Schulte, A.; Schuhmann, W. Constant-Distance Mode Scanning Electrochemical Microscopy (SECM)—Part I: Adaptation of a Non-Optical Shear-Force-Based Positioning Mode for SECM Tips. *Chem. A Eur. J.* **2003**, *9*, 2025–2033. [CrossRef] [PubMed]
36. Comstock, D.J.; Elam, J.W.; Pellin, M.J.; Hersam, M.C. Integrated Ultramicroelectrode−Nanopipet Probe for Concurrent Scanning Electrochemical Microscopy and Scanning Ion Conductance Microscopy. *Anal. Chem.* **2010**, *82*, 1270–1276. [CrossRef] [PubMed]
37. Takahashi, Y.; Shevchuk, A.I.; Novak, P.; Murakami, Y.; Shiku, H.; Korchev, Y.E.; Matsue, T. Simultaneous Noncontact Topography and Electrochemical Imaging by SECM/SICM Featuring Ion Current Feedback Regulation. *J. Am. Chem. Soc.* **2010**, *132*, 10118–10126. [CrossRef] [PubMed]
38. Gardner, C.E.; Macpherson, J. V Peer Reviewed: Atomic Force Microscopy Probes Go Electrochemical. *Anal. Chem.* **2002**, *74*, 576A–584A. [CrossRef] [PubMed]
39. Velmurugan, J.; Agrawal, A.; An, S.; Choudhary, E.; Szalai, V.A. Fabrication of Scanning Electrochemical Microscopy-Atomic Force Microscopy Probes to Image Surface Topography and Reactivity at the Nanoscale. *Anal. Chem.* **2017**, *89*, 2687–2691. [CrossRef] [PubMed]

40. Seifert, J.; Rheinlaender, J.; Novak, P.; Korchev, Y.E.; Schäffer, T.E. Comparison of Atomic Force Microscopy and Scanning Ion Conductance Microscopy for Live Cell Imaging. *Langmuir* **2015**, *31*, 6807–6813. [CrossRef] [PubMed]
41. Liu, Y.; Holzinger, A.; Knittel, P.; Poltorak, L.; Gamero-Quijano, A.; Rickard, W.D.A.; Walcarius, A.; Herzog, G.; Kranz, C.; Arrigan, D.W.M. Visualization of Diffusion within Nanoarrays. *Anal. Chem.* **2016**, *88*, 6689–6695. [CrossRef] [PubMed]
42. Barker, A.L.; Unwin, P.R.; Gardner, J.W.; Rieley, H. A multi-electrode probe for parallel imaging in scanning electrochemical microscopy. *Electrochem. Commun.* **2004**, *6*, 91–97. [CrossRef]
43. Cortés-Salazar, F.; Momotenko, D.; Girault, H.H.; Lesch, A.; Wittstock, G. Seeing Big with Scanning Electrochemical Microscopy. *Anal. Chem.* **2011**, *83*, 1493–1499. [CrossRef] [PubMed]
44. Lin, T.-E.; Lesch, A.; Li, C.-L.; Girault, H.H. Mapping the antioxidant activity of apple peels with soft probe scanning electrochemical microscopy. *J. Electroanal. Chem.* **2017**, *786*, 120–128. [CrossRef]
45. Lesch, A.; Momotenko, D.; Cortés-Salazar, F.; Roelfs, F.; Girault, H.H.; Wittstock, G. High-throughput scanning electrochemical microscopy brushing of strongly tilted and curved surfaces. *Electrochim. Acta* **2013**, *110*, 30–41. [CrossRef]
46. Lesch, A.; Chen, P.-C.; Roelfs, F.; Dosche, C.; Momotenko, D.; Cortés-Salazar, F.; Girault, H.H.; Wittstock, G. Finger Probe Array for Topography-Tolerant Scanning Electrochemical Microscopy of Extended Samples. *Anal. Chem.* **2014**, *86*, 713–720. [CrossRef] [PubMed]
47. Lin, T.E.; Lu, Y.J.; Sun, C.L.; Pick, H.; Chen, J.P.; Lesch, A.; Girault, H.H. Soft Electrochemical Probes for Mapping the Distribution of Biomarkers and Injected Nanomaterials in Animal and Human Tissues. *Angew. Chem. Int. Ed.* **2017**, *56*, 16498–16502. [CrossRef] [PubMed]
48. Clausmeyer, J.; Schuhmann, W. Nanoelectrodes: Applications in electrocatalysis, single-cell analysis and high-resolution electrochemical imaging. *TrAC Trends Anal. Chem.* **2016**, *79*, 46–59. [CrossRef]
49. Nioradze, N.; Chen, R.; Kim, J.; Shen, M.; Santhosh, P.; Amemiya, S. Origins of Nanoscale Damage to Glass-Sealed Platinum Electrodes with Submicrometer and Nanometer Size. *Anal. Chem.* **2013**, *85*, 6198–6202. [CrossRef] [PubMed]
50. Chen, R.; Hu, K.; Yu, Y.; Mirkin, M.V.; Amemiya, S. Focused-Ion-Beam-Milled Carbon Nanoelectrodes for Scanning Electrochemical Microscopy. *J. Electrochem. Soc.* **2016**, *163*, H3032–H3037. [CrossRef] [PubMed]
51. Kim, J.; Shen, M.; Nioradze, N.; Amemiya, S. Stabilizing Nanometer Scale Tip-to-Substrate Gaps in Scanning Electrochemical Microscopy Using an Isothermal Chamber for Thermal Drift Suppression. *Anal. Chem.* **2012**, *84*, 3489–3492. [CrossRef] [PubMed]
52. Kim, J.; Renault, C.; Nioradze, N.; Arroyo-Currás, N.; Leonard, K.C.; Bard, A.J. Nanometer Scale Scanning Electrochemical Microscopy Instrumentation. *Anal. Chem.* **2016**, *88*, 10284–10289. [CrossRef] [PubMed]
53. Sun, T.; Yu, Y.; Zacher, B.J.; Mirkin, M. V Scanning Electrochemical Microscopy of Individual Catalytic Nanoparticles. *Angew. Chem. Int. Ed.* **2014**, *53*, 14120–14123. [CrossRef] [PubMed]
54. Kim, J.; Renault, C.; Nioradze, N.; Arroyo-Currás, N.; Leonard, K.C.; Bard, A.J. Electrocatalytic Activity of Individual Pt Nanoparticles Studied by Nanoscale Scanning Electrochemical Microscopy. *J. Am. Chem. Soc.* **2016**, *138*, 8560–8568. [CrossRef] [PubMed]
55. Chen, R.; Balla, R.J.; Lima, A.; Amemiya, S. Characterization of Nanopipet-Supported ITIES Tips for Scanning Electrochemical Microscopy of Single Solid-State Nanopores. *Anal. Chem.* **2017**, *89*, 9946–9952. [CrossRef] [PubMed]
56. Wang, Y.; Kececi, K.; Velmurugan, J.; Mirkin, M. V Electron transfer/ion transfer mode of scanning electrochemical microscopy (SECM): A new tool for imaging and kinetic studies. *Chem. Sci.* **2013**, *4*, 3606–3616. [CrossRef]
57. Hansma, P.K.; Drake, B.; Marti, O.; Gould, S.A.; Prater, C.B. The scanning ion-conductance microscope. *Science* **1989**, *243*, 641–643. [CrossRef] [PubMed]
58. Rheinlaender, J.; Schäffer, T.E. Lateral Resolution and Image Formation in Scanning Ion Conductance Microscopy. *Anal. Chem.* **2015**, *87*, 7117–7124. [CrossRef] [PubMed]
59. Nakajima, M.; Mizutani, Y.; Iwata, F.; Ushiki, T. Scanning ion conductance microscopy for visualizing the three-dimensional surface topography of cells and tissues. *Semin. Cell Dev. Biol.* **2018**, *73*, 125–131. [CrossRef] [PubMed]

60. Momotenko, D.; McKelvey, K.; Kang, M.; Meloni, G.N.; Unwin, P.R. Simultaneous Interfacial Reactivity and Topography Mapping with Scanning Ion Conductance Microscopy. *Anal. Chem.* **2016**, *88*, 2838–2846. [CrossRef] [PubMed]
61. McKelvey, K.; Kinnear, S.L.; Perry, D.; Momotenko, D.; Unwin, P.R. Surface Charge Mapping with a Nanopipette. *J. Am. Chem. Soc.* **2014**, *136*, 13735–13744. [CrossRef] [PubMed]
62. McKelvey, K.; Perry, D.; Byers, J.C.; Colburn, A.W.; Unwin, P.R. Bias Modulated Scanning Ion Conductance Microscopy. *Anal. Chem.* **2014**, *86*, 3639–3646. [CrossRef] [PubMed]
63. Chen, C.-C.; Baker, L.A. Effects of pipette modulation and imaging distances on ion currents measured with Scanning Ion Conductance Microscopy (SICM). *Analyst* **2011**, *136*, 90–97. [CrossRef] [PubMed]
64. Perry, D.; Page, A.; Chen, B.; Frenguelli, B.G.; Unwin, P.R. Differential-Concentration Scanning Ion Conductance Microscopy. *Anal. Chem.* **2017**, *89*, 12458–12465. [CrossRef] [PubMed]
65. Thakar, R.; Weber, A.E.; Morris, C.A.; Baker, L.A. Multifunctional carbon nanoelectrodes fabricated by focused ion beam milling. *Analyst* **2013**, *138*, 5973–5982. [CrossRef] [PubMed]
66. Lazenby, R.A.; McKelvey, K.; Peruffo, M.; Baghdadi, M.; Unwin, P.R. Nanoscale intermittent contact-scanning electrochemical microscopy. *J. Solid State Electrochem.* **2013**, *17*, 2979–2987. [CrossRef]
67. Takahashi, Y.; Shevchuk, A.I.; Novak, P.; Zhang, Y.; Ebejer, N.; Macpherson, J.V.; Unwin, P.R.; Pollard, A.J.; Roy, D.; Clifford, C.A.; et al. Multifunctional Nanoprobes for Nanoscale Chemical Imaging and Localized Chemical Delivery at Surfaces and Interfaces. *Angew. Chem. Int. Ed.* **2011**, *50*, 9638–9642. [CrossRef] [PubMed]
68. Shi, W.; Sa, N.; Thakar, R.; Baker, L.A. Nanopipette delivery: Influence of surface charge. *Analyst* **2015**, *140*, 4835–4842. [CrossRef] [PubMed]
69. Page, A.; Kang, M.; Armitstead, A.; Perry, D.; Unwin, P.R. Quantitative Visualization of Molecular Delivery and Uptake at Living Cells with Self-Referencing Scanning Ion Conductance Microscopy-Scanning Electrochemical Microscopy. *Anal. Chem.* **2017**, *89*, 3021–3028. [CrossRef] [PubMed]
70. Perry, D.; Momotenko, D.; Lazenby, R.A.; Kang, M.; Unwin, P.R. Characterization of Nanopipettes. *Anal. Chem.* **2016**, *88*, 5523–5530. [CrossRef] [PubMed]
71. Tognoni, E.; Baschieri, P.; Ascoli, C.; Pellegrini, M.; Pellegrino, M. Characterization of tip size and geometry of the pipettes used in scanning ion conductance microscopy. *Micron* **2016**, *83*, 11–18. [CrossRef] [PubMed]
72. Actis, P.; Tokar, S.; Clausmeyer, J.; Babakinejad, B.; Mikhaleva, S.; Cornut, R.; Takahashi, Y.; López Córdoba, A.; Novak, P.; Shevchuck, A.I.; et al. Electrochemical Nanoprobes for Single-Cell Analysis. *ACS Nano* **2014**, *8*, 875–884. [CrossRef] [PubMed]
73. Hu, K.; Gao, Y.; Wang, Y.; Yu, Y.; Zhao, X.; Rotenberg, S.A.; Gökmeşe, E.; Mirkin, M.V.; Friedman, G.; Gogotsi, Y. Platinized carbon nanoelectrodes as potentiometric and amperometric SECM probes. *J. Solid State Electrochem.* **2013**, *17*, 2971–2977. [CrossRef]
74. O'Connell, M.A.; Lewis, J.R.; Wain, A.J. Electrochemical imaging of hydrogen peroxide generation at individual gold nanoparticles. *Chem. Commun.* **2015**, *51*, 10314–10317. [CrossRef] [PubMed]
75. Şen, M.; Takahashi, Y.; Matsumae, Y.; Horiguchi, Y.; Kumatani, A.; Ino, K.; Shiku, H.; Matsue, T. Improving the Electrochemical Imaging Sensitivity of Scanning Electrochemical Microscopy-Scanning Ion Conductance Microscopy by Using Electrochemical Pt Deposition. *Anal. Chem.* **2015**, *87*, 3484–3489. [CrossRef] [PubMed]
76. Justino, C.I.L.; Rocha-Santos, T.A.; Duarte, A.C.; Rocha-Santos, T.A. Review of analytical figures of merit of sensors and biosensors in clinical applications. *TrAC Trends Anal. Chem.* **2010**, *29*, 1172–1183. [CrossRef]
77. Ganesana, M.; Lee, S.T.; Wang, Y.; Venton, B.J. Analytical Techniques in Neuroscience: Recent Advances in Imaging, Separation, and Electrochemical Methods. *Anal. Chem.* **2017**, *89*, 314–341. [CrossRef] [PubMed]
78. Huffman, M.L.; Venton, B.J. Carbon-Fiber Microelectrodes for In Vivo Applications. *Analyst* **2009**, *134*, 18–24. [CrossRef] [PubMed]
79. Ha, Y.; Myung, D.; Shim, J.H.; Kim, M.H.; Lee, Y. A dual electrochemical microsensor for simultaneous imaging of oxygen and pH over the rat kidney surface. *Analyst* **2013**, *138*, 5258–5264. [CrossRef] [PubMed]
80. Nadappuram, B.P.; McKelvey, K.; Al Botros, R.; Colburn, A.W.; Unwin, P.R. Fabrication and Characterization of Dual Function Nanoscale pH-Scanning Ion Conductance Microscopy (SICM) Probes for High Resolution pH Mapping. *Anal. Chem.* **2013**, *85*, 8070–8074. [CrossRef] [PubMed]
81. Lin, T.-E.; Cortés-Salazar, F.; Lesch, A.; Qiao, L.; Bondarenko, A.; Girault, H.H. Multiple scanning electrochemical microscopy mapping of tyrosinase in micro-contact printed fruit samples on polyvinylidene fluoride membrane. *Electrochim. Acta* **2015**, *179*, 57–64. [CrossRef]

82. Horrocks, B.R.; Schmidtke, D.; Heller, A.; Bard, A.J. Scanning electrochemical microscopy. 24. Enzyme ultramicroelectrodes for the measurement of hydrogen peroxide at surfaces. *Anal. Chem.* **1993**, *65*, 3605–3614. [CrossRef] [PubMed]
83. Polcari, D.; Kwan, A.; Van Horn, M.R.; Danis, L.; Pollegioni, L.; Ruthazer, E.S.; Mauzeroll, J. Disk-Shaped Amperometric Enzymatic Biosensor for in Vivo Detection of D-serine. *Anal. Chem.* **2014**, *86*, 3501–3507. [CrossRef] [PubMed]
84. Polcari, D.; Perry, S.C.; Pollegioni, L.; Geissler, M.; Mauzeroll, J. Localized Detection of D-Serine by using an Enzymatic Amperometric Biosensor and Scanning Electrochemical Microscopy. *ChemElectroChem* **2017**, *4*, 920–926. [CrossRef]
85. Ciobanu, M.; Taylor, D.E.; Wilburn, J.P.; Cliffel, D.E. Glucose and Lactate Biosensors for Scanning Electrochemical Microscopy Imaging of Single Live Cells. *Anal. Chem.* **2008**, *80*, 2717–2727. [CrossRef] [PubMed]
86. Lugo-Morales, L.Z.; Loziuk, P.L.; Corder, A.K.; Toups, J.V.; Roberts, J.G.; McCaffrey, K.A.; Sombers, L.A. Enzyme-Modified Carbon-Fiber Microelectrode for the Quantification of Dynamic Fluctuations of Nonelectroactive Analytes Using Fast-Scan Cyclic Voltammetry. *Anal. Chem.* **2013**, *85*, 8780–8786. [CrossRef] [PubMed]
87. Soldà, A.; Valenti, G.; Marcaccio, M.; Giorgio, M.; Pelicci, P.G.; Paolucci, F.; Rapino, S. Glucose and Lactate Miniaturized Biosensors for SECM-Based High-Spatial Resolution Analysis: A Comparative Study. *ACS Sens.* **2017**, *2*, 1310–1318. [CrossRef] [PubMed]
88. Creager, S.E.; Olsen, K.G. Self-assembled monolayers and enzyme electrodes: Progress, problems and prospects. *Anal. Chim. Acta* **1995**, *307*, 277–289. [CrossRef]
89. Zhao, F.; Conzuelo, F.; Hartmann, V.; Li, H.; Stapf, S.; Nowaczyk, M.M.; Rögner, M.; Plumeré, N.; Lubitz, W.; Schuhmann, W. A novel versatile microbiosensor for local hydrogen detection by means of scanning photoelectrochemical microscopy. *Biosens. Bioelectron.* **2017**, *94*, 433–437. [CrossRef] [PubMed]
90. Wilburn, J.P.; Ciobanu, M.; Cliffel, D.E. Scanning Electrochemical Microscopy of Individual Pancreatic Islets. *J. Electrochem. Soc.* **2016**, *163*, H3077–H3082. [CrossRef]
91. Liu, J.; Wagan, S.; Dávila Morris, M.; Taylor, J.; White, R.J. Achieving Reproducible Performance of Electrochemical, Folding Aptamer-Based Sensors on Microelectrodes: Challenges and Prospects. *Anal. Chem.* **2014**, *86*, 11417–11424. [CrossRef] [PubMed]
92. Das, J.; Kelley, S.O. Tuning the Bacterial Detection Sensitivity of Nanostructured Microelectrodes. *Anal. Chem.* **2013**, *85*, 7333–7338. [CrossRef] [PubMed]
93. Wei, C.; Bard, A.J.; Nagy, G.; Toth, K. Scanning Electrochemical Microscopy. 28. Ion-Selective Neutral Carrier-Based Microelectrode Potentiometry. *Anal. Chem.* **1995**, *67*, 1346–1356. [CrossRef]
94. Izquierdo, J.; Kiss, A.; Santana, J.J.; Nagy, L.; Bitter, I.; Isaacs, H.S.; Nagy, G.; Souto, R.M. Development of Mg^{2+} Ion-Selective Microelectrodes for Potentiometric Scanning Electrochemical Microscopy Monitoring of Galvanic Corrosion Processes. *J. Electrochem. Soc.* **2013**, *160*, C451–C459. [CrossRef]
95. Ummadi, J.G.; Downs, C.J.; Joshi, V.S.; Ferracane, J.L.; Koley, D. Carbon-Based Solid-State Calcium Ion-Selective Microelectrode and Scanning Electrochemical Microscopy: A Quantitative Study of pH-Dependent Release of Calcium Ions from Bioactive Glass. *Anal. Chem.* **2016**, *88*, 3218–3226. [CrossRef] [PubMed]
96. Filotás, D.; Asserghine, A.; Nagy, L.; Nagy, G. Short-term influence of interfering ion activity change on ion-selective micropipette electrode potential; another factor that can affect the time needed for imaging in potentiometric SECM. *Electrochem. Commun.* **2017**, *77*, 62–64. [CrossRef]
97. Kiss, A.; Nagy, G. Deconvolution of potentiometric SECM images recorded with high scan rate. *Electrochim. Acta* **2015**, *163*, 303–309. [CrossRef]
98. Yamada, H.; Haraguchi, D.; Yasunaga, K. Fabrication and characterization of a K^+-selective nanoelectrode and simultaneous imaging of topography and local K^+ flux using scanning electrochemical microscopy. *Anal. Chem.* **2014**, *86*, 8547–8552. [CrossRef] [PubMed]
99. Nascimento, R.A.S.; Özel, R.E.; Mak, W.H.; Mulato, M.; Singaram, B.; Pourmand, N. Single Cell "Glucose Nanosensor" Verifies Elevated Glucose Levels in Individual Cancer Cells. *Nano Lett.* **2016**, *16*, 1194–1200. [CrossRef] [PubMed]
100. Vilozny, B.; Actis, P.; Seger, R.A.; Vallmajo-Martin, Q.; Pourmand, N. Reversible Cation Response with a Protein-Modified Nanopipette. *Anal. Chem.* **2011**, *83*, 6121–6126. [CrossRef] [PubMed]

101. Actis, P.; Mak, A.C.; Pourmand, N. Functionalized nanopipettes: Toward label-free, single cell biosensors. *Bioanal. Rev.* **2010**, *1*, 177–185. [CrossRef] [PubMed]
102. Umehara, S.; Karhanek, M.; Davis, R.W.; Pourmand, N. Label-free biosensing with functionalized nanopipette probes. *Proc. Natl. Acad. Sci. USA* **2009**, *106*, 4611–4616. [CrossRef] [PubMed]
103. Actis, P.; Rogers, A.; Nivala, J.; Vilozny, B.; Seger, R.A.; Jejelowo, O.; Pourmand, N. Reversible thrombin detection by aptamer functionalized STING sensors. *Biosens. Bioelectron.* **2011**, *26*, 4503–4507. [CrossRef] [PubMed]
104. Shi, W.; Friedman, A.K.; Baker, L.A. Nanopore Sensing. *Anal. Chem.* **2017**, *89*, 157–188. [CrossRef] [PubMed]
105. Coronado, R.; Latorre, R. Phospholipid bilayers made from monolayers on patch-clamp pipettes. *Biophys. J.* **1983**, *43*, 231–236. [CrossRef]
106. Alvarez, O. Ion Channel Reconstitution. In *Ion Channel Reconstitution*; Miller, C., Ed.; Springer: New York, NY, USA, 1986; pp. 115–130. ISBN 978-1-4757-1363-3.
107. Zhou, Y.; Bright, L.K.; Shi, W.; Aspinwall, C.A.; Baker, L.A. Ion Channel Probes for Scanning Ion Conductance Microscopy. *Langmuir* **2014**, *30*, 15351–15355. [CrossRef] [PubMed]
108. Macazo, F.C.; White, R.J. Bioinspired Protein Channel-Based Scanning Ion Conductance Microscopy (Bio-SICM) for Simultaneous Conductance and Specific Molecular Imaging. *J. Am. Chem. Soc.* **2016**, *138*, 2793–2801. [CrossRef] [PubMed]
109. Shi, W.; Zeng, Y.; Zhou, L.; Xiao, Y.; Cummins, T.R.; Baker, L.A. Membrane patches as ion channel probes for scanning ion conductance microscopy. *Faraday Discuss.* **2016**, *193*, 81–97. [CrossRef] [PubMed]
110. Lazenby, R.A.; Macazo, F.C.; Wormsbecher, R.F.; White, R.J. Quantitative Framework for Stochastic Nanopore Sensors Using Multiple Channels. *Anal. Chem.* **2018**, *90*, 903–911. [CrossRef] [PubMed]
111. Bayley, H.; Braha, O.; Gu, L.Q. Stochastic sensing with protein pores. *Adv. Mater.* **2000**, *12*, 139–142. [CrossRef]
112. Shi, W.; Zeng, Y.; Zhu, C.; Xiao, Y.; Cummins, T.R.; Hou, J.; Baker, L.A. Characterization of Membrane Patch-Ion Channel Probes for Scanning Ion Conductance Microscopy. *Small* **2018**, *14*, 1702945. [CrossRef] [PubMed]
113. Macazo, F.C.; White, R.J. Monitoring Charge Flux to Quantify Unusual Ligand-Induced Ion Channel Activity for Use in Biological Nanopore-Based Sensors. *Anal. Chem.* **2014**, *86*, 5519–5525. [CrossRef] [PubMed]
114. Novak, P.; Li, C.; Shevchuk, A.I.; Stepanyan, R.; Caldwell, M.; Hughes, S.; Smart, T.G.; Gorelik, J.; Ostanin, V.P.; Lab, M.J.; et al. Nanoscale live-cell imaging using hopping probe ion conductance microscopy. *Nat. Methods* **2009**, *6*, 279–281. [CrossRef] [PubMed]
115. Lazenby, R.A.; McKelvey, K.; Unwin, P.R. Hopping intermittent contact-scanning electrochemical microscopy (HIC-SECM): Visualizing interfacial reactions and fluxes from surfaces to bulk solution. *Anal. Chem.* **2013**, *85*, 2937–2944. [CrossRef] [PubMed]
116. Nebel, M.; Eckhard, K.; Erichsen, T.; Schulte, A.; Schuhmann, W. 4D Shearforce-Based Constant-Distance Mode Scanning Electrochemical Microscopy. *Anal. Chem.* **2010**, *82*, 7842–7848. [CrossRef] [PubMed]
117. Li, M.S.M.; Filice, F.P.; Ding, Z. Determining live cell topography by scanning electrochemical microscopy. *J. Electroanal. Chem.* **2016**, *779*, 176–186. [CrossRef]
118. Filice, F.P.; Li, M.S.M.; Henderson, J.D.; Ding, Z. Mapping Cd^{2+}-induced membrane permeability changes of single live cells by means of scanning electrochemical microscopy. *Anal. Chim. Acta* **2016**, *908*, 85–94. [CrossRef] [PubMed]
119. Henderson, J.D.; Filice, F.P.; Li, M.S.M.; Ding, Z. Tracking live cell response to cadmium (II) concentrations by scanning electrochemical microscopy. *J. Inorg. Biochem.* **2016**, *158*, 92–98. [CrossRef] [PubMed]
120. Kuss, S.; Trinh, D.; Mauzeroll, J. High-Speed Scanning Electrochemical Microscopy Method for Substrate Kinetic Determination: Application to Live Cell Imaging in Human Cancer. *Anal. Chem.* **2015**, *87*, 8102–8106. [CrossRef] [PubMed]
121. Kuss, S.; Trinh, D.; Danis, L.; Mauzeroll, J. High-Speed Scanning Electrochemical Microscopy Method for Substrate Kinetic Determination: Method and Theory. *Anal. Chem.* **2015**, *87*, 8096–8101. [CrossRef] [PubMed]
122. Kuss, S.; Kuss, C.; Trinh, D.; Schougaard, S.B.; Mauzeroll, J. Forced convection during scanning electrochemical microscopy imaging over living cells: Effect of topographies and kinetics on the microelectrode current. *Electrochim. Acta* **2013**, *110*, 42–48. [CrossRef]

123. Ida, H.; Takahashi, Y.; Kumatani, A.; Shiku, H.; Matsue, T. High Speed Scanning Ion Conductance Microscopy for Quantitative Analysis of Nanoscale Dynamics of Microvilli. *Anal. Chem.* **2017**, *89*, 6015–6020. [CrossRef] [PubMed]
124. Kiss, A.; Nagy, G. New SECM scanning algorithms for improved potentiometric imaging of circularly symmetric targets. *Electrochim. Acta* **2014**, *119*, 169–174. [CrossRef]
125. Zhuang, J.; Jiao, Y.; Mugabo, V. A new scanning mode to improve scanning ion conductance microscopy imaging rate with pipette predicted movement. *Micron* **2017**, *101*, 177–185. [CrossRef] [PubMed]
126. Ebejer, N.; Schnippering, M.; Colburn, A.W.; Edwards, M.A.; Unwin, P.R. Localized High Resolution Electrochemistry and Multifunctional Imaging: Scanning Electrochemical Cell Microscopy. *Anal. Chem.* **2010**, *82*, 9141–9145. [CrossRef] [PubMed]
127. Bentley, C.L.; Kang, M.; Unwin, P.R. Nanoscale Structure Dynamics within Electrocatalytic Materials. *J. Am. Chem. Soc.* **2017**, *139*, 16813–16821. [CrossRef] [PubMed]
128. Bentley, C.L.; Kang, M.; Maddar, F.M.; Li, F.; Walker, M.; Zhang, J.; Unwin, P.R. Electrochemical maps and movies of the hydrogen evolution reaction on natural crystals of molybdenite (MoS_2): Basal vs. edge plane activity. *Chem. Sci.* **2017**, *8*, 6583–6593. [CrossRef] [PubMed]
129. Momotenko, D.; Byers, J.C.; McKelvey, K.; Kang, M.; Unwin, P.R. High-Speed Electrochemical Imaging. *ACS Nano* **2015**, *9*, 8942–8952. [CrossRef] [PubMed]
130. Wang, J.; Trouillon, R.; Lin, Y.; Svensson, M.I.; Ewing, A.G. Individually Addressable Thin-Film Ultramicroelectrode Array for Spatial Measurements of Single Vesicle Release. *Anal. Chem.* **2013**, *85*, 5600–5608. [CrossRef] [PubMed]
131. Wang, J.; Trouillon, R.; Dunevall, J.; Ewing, A.G. Spatial Resolution of Single-Cell Exocytosis by Microwell-Based Individually Addressable Thin Film Ultramicroelectrode Arrays. *Anal. Chem.* **2014**, *86*, 4515–4520. [CrossRef] [PubMed]
132. Wigström, J.; Dunevall, J.; Najafinobar, N.; Lovrić, J.; Wang, J.; Ewing, A.G.; Cans, A.-S. Lithographic Microfabrication of a 16-Electrode Array on a Probe Tip for High Spatial Resolution Electrochemical Localization of Exocytosis. *Anal. Chem.* **2016**, *88*, 2080–2087. [CrossRef] [PubMed]
133. Schierbaum, N.; Hack, M.; Betz, O.; Schäffer, T.E. Macro-SICM: A Scanning Ion Conductance Microscope for Large-Range Imaging. *Anal. Chem.* **2018**. [CrossRef] [PubMed]
134. Abe, H.; Ino, K.; Li, C.-Z.; Kanno, Y.; Inoue, K.Y.; Suda, A.; Kunikata, R.; Matsudaira, M.; Takahashi, Y.; Shiku, H.; et al. Electrochemical Imaging of Dopamine Release from Three-Dimensional-Cultured PC12 Cells Using Large-Scale Integration-Based Amperometric Sensors. *Anal. Chem.* **2015**, *87*, 6364–6370. [CrossRef] [PubMed]
135. Ino, K.; Sen, M.; Shiku, H.; Matsue, T. Micro/nanoelectrochemical probe and chip devices for evaluation of three-dimensional cultured cells. *Analyst* **2017**, *142*, 4343–4354. [CrossRef] [PubMed]
136. Kanno, Y.; Ino, K.; Abe, H.; Sakamoto, C.; Onodera, T.; Inoue, K.Y.; Suda, A.; Kunikata, R.; Matsudaira, M.; Shiku, H.; et al. Electrochemicolor Imaging Using an LSI-Based Device for Multiplexed Cell Assays. *Anal. Chem.* **2017**, *89*, 12778–12786. [CrossRef] [PubMed]
137. Kara, A.; Reitz, A.; Mathault, J.; Mehou-Loko, S.; Amirdehi, M.A.; Miled, A.; Greener, J. Electrochemical imaging for microfluidics: A full-system approach. *Lab Chip* **2016**, *16*, 1081–1087. [CrossRef] [PubMed]
138. Wydallis, J.B.; Feeny, R.M.; Wilson, W.; Kern, T.; Chen, T.; Tobet, S.; Reynolds, M.M.; Henry, C.S. Spatiotemporal norepinephrine mapping using a high-density CMOS microelectrode array. *Lab Chip* **2015**, *15*, 4075–4082. [CrossRef] [PubMed]
139. Mensack, M.M.; Wydallis, J.B.; Lynn, N.S.; Dandy, D.S.; Henry, C.S. Spatially resolved electrochemical sensing of chemical gradients. *Lab Chip* **2013**, *13*, 208–211. [CrossRef] [PubMed]
140. Chung, J.E.; Joo, H.R.; Fan, J.L.; Liu, D.F.; Barnett, A.H.; Chen, S.; Geaghan-Breiner, C.; Karlsson, M.P.; Karlsson, M.; Lee, K.Y.; et al. High-density, long-lasting, and multi-region electrophysiological recordings using polymer electrode arrays. *bioRxiv* **2018**, 242693. [CrossRef]
141. Szostak, K.M.; Grand, L.; Constandinou, T.G. Neural interfaces for intracortical recording: Requirements, fabrication methods, and characteristics. *Front. Neurosci.* **2017**, *11*, 665. [CrossRef] [PubMed]
142. Felix, S.H.; Shah, K.G.; Tolosa, V.M.; Sheth, H.J.; Tooker, A.C.; Delima, T.L.; Jadhav, S.P.; Frank, L.M.; Pannu, S.S. Insertion of Flexible Neural Probes Using Rigid Stiffeners Attached with Biodissolvable Adhesive. *J. Vis. Exp.* **2013**, *79*, e50609. [CrossRef] [PubMed]

143. Tseng, T.T.-C.; Monbouquette, H.G. Implantable microprobe with arrayed microsensors for combined amperometric monitoring of the neurotransmitters, glutamate and dopamine. *J. Electroanal. Chem.* **2012**, *682*, 141–146. [CrossRef] [PubMed]
144. Şen, M.; Ino, K.; Inoue, K.Y.; Arai, T.; Nishijo, T.; Suda, A.; Kunikata, R.; Shiku, H.; Matsue, T. LSI-based amperometric sensor for real-time monitoring of embryoid bodies. *Biosens. Bioelectron.* **2013**, *48*, 12–18. [CrossRef] [PubMed]
145. Kanno, Y.; Ino, K.; Inoue, K.Y.; Şen, M.; Suda, A.; Kunikata, R.; Matsudaira, M.; Abe, H.; Li, C.-Z.; Shiku, H.; et al. Feedback mode-based electrochemical imaging of conductivity and topography for large substrate surfaces using an LSI-based amperometric chip device with 400 sensors. *J. Electroanal. Chem.* **2015**, *741*, 109–113. [CrossRef]
146. Kanno, Y.; Ino, K.; Sakamoto, C.; Inoue, K.Y.; Matsudaira, M.; Suda, A.; Kunikata, R.; Ishikawa, T.; Abe, H.; Shiku, H.; et al. Potentiometric bioimaging with a large-scale integration (LSI)-based electrochemical device for detection of enzyme activity. *Biosens. Bioelectron.* **2016**, *77*, 709–714. [CrossRef] [PubMed]
147. Kim, B.N.; Herbst, A.D.; Kim, S.J.; Minch, B.A.; Lindau, M. Parallel recording of neurotransmitters release from chromaffin cells using a 10 × 10 CMOS IC potentiostat array with on-chip working electrodes. *Biosens. Bioelectron.* **2013**, *41*, 736–744. [CrossRef] [PubMed]